International Journal of Solids and Structures 69–70 (2015) 45–59

Contents lists available at ScienceDirect

International Journal of Solids and Structures

journal homepage: www.elsevier.com/locate/ijsolstr

Sensitivity of the thermomechanical response of elastic structures to microstructural changes

Víctor D. Fachinotti [a,*], Sebastián Toro [a], Pablo J. Sánchez [a,c], Alfredo E. Huespe [a,b]

[a] Centro de Investigación de Métodos Computacionales (CIMEC), Universidad Nacional del Litoral (UNL)/Consejo Nacional de Investigaciones Científicas y Técnicas (CONICET), Predio CCT-CONICET Santa Fe, Ruta 168, Paraje El Pozo, 3000 Santa Fe, Argentina
[b] International Center for Numerical Methods in Engineering (CIMNE), Campus Nord UPC, Edifici C-1, c/Jordi Girona 1-3, 08034 Barcelona, Spain
[c] Grupo de Investigación en Métodos Numéricos en Ingeniería (GIMNI), Universidad Tecnológica Nacional (UTN), Facultad Regional Santa Fe, Lavaise 610, 3000 Santa Fe, Argentina

ARTICLE INFO

Article history:
Received 26 July 2014
Received in revised form 14 May 2015
Available online 18 June 2015

Keywords:
Microstructural material design
Structural optimization
Sensitivity to microstructural changes
Computational homogenization of materials
Response surface methodology

ABSTRACT

This paper is focused on the analysis of the sensitivity of the thermomechanical response of a macroscopic elastic body to changes that occur at the microstructure. This problem is a key issue in material design.

The sensitivity analysis relies on an accurate determination of the effective properties of the heterogeneous material. These effective properties are determined by computational homogenization. And their sensitivities, with respect to the parameters defining the microstructure, are then computed.

For an efficient evaluation of the thermomechanical response, we propose to build response surfaces for the effective material properties. The surfaces are generated in an offline stage, by solving a series of homogenization problems at the microscale. In such a way, the fully online multiscale response analysis reduces to a standard problem at the macroscale. Thus, an important reduction in computational time is achieved, which is a crucial advantage for material design.

The capability of the proposed methodology is shown in light of its application to the design of a thermally-loaded structure with variable microstructure. Considerable improvements in the structural response are achieved.

1. Introduction

As stated by Torquato (2010), the deep knowledge of the sensitivity of the observable macroscopic response of a body to changes in the structure of its constituent material at one or more subscales is the holy grail of materials science. Traditionally, the engineers used to choose from a catalog the best material to build a structure or mechanism with a desired response. In recent years, thanks to the ever-growing power of computers and the maturity of Computational Multiscale Modeling (CMM), an alternative approach is emerging, specially for high-performance applications: the Materials by Design (MbD) approach (McDowell and Story, 1998). MbD consists in designing the structure of a material at a subscale in order to make this material (or the body made of this material) the best-suited for a specific application.

In general, the term subscale refers to a wide range of length scales, from atomistic or molecular to microscopic and mesoscopic, whenever the length scale be much smaller than the dimensions of the structure made of the considered material. This paper is focused on the design of heterogeneous materials, typically composites, by altering their structure at one (and only one) subscale where the material can still be assumed to be a continuum. For the sake of convenience, let us refer to the material at such scale as "microstructure".

Further, we are currently interested in "quantitatively characterized" materials (Kachanov and Sevostianov, 2005), those whose macroscopic or effective physical properties can be expressed as functions of identified microstructural parameters: e.g., fiber orientation in fiber-reinforced polymers (Lund and Stegmann, 2005), density and irregularity factors in materials with isolated inhomogeneities (Kachanov and Sevostianov, 2005; Tsukrov and Kachanov, 2000), size of particles or beads in coating of dental implants (Rungsiyakull et al., 2010; Chen et al., 2013).

From the computational point of view, MbD can be formulated as a structural optimization problem where the cost function is defined at the macrostructure level. The goal is to obtain the distribution of microstructures along the macrostructure domain providing the minimum cost. This approach has been addressed by Rodrigues et al. (2002) and Bendsøe and Sigmund (2003). The so-determined material can be seen as a functionally graded material (FGM) in the sense that the microstructure changes smoothly

* Corresponding author.
E-mail address: vfachino@intec.unl.edu.ar (V.D. Fachinotti).

http://dx.doi.org/10.1016/j.ijsolstr.2015.06.009
0020-7683/

from point to point at the macroscale. Paulino et al. (2009) have studied the microstructural optimization problem for a FGM.

Based on this MbD paradigm, the key point for developing an admissible computational procedure relies on the concept of hierarchical optimization (Rodrigues et al., 2002): the microstructural design problem (the *inner problem*) is uncoupled from the problem of finding the minimum cost function at the macroscale (the *outer problem*). Then, the sensitivity analysis addressed in this work plays an extremely important role during the process of obtaining the minimum cost function of the outer problem.

In our case, the inner problem consists on determining the way the effective properties of quantitatively characterized materials depend on microstructural parameters. In order to solve this problem, recourse can be made to experiments (the most expensive option), homogenization techniques for specific materials having simple microstructural topologies like analytical solutions (Kachanov and Sevostianov, 2005; Tsukrov and Kachanov, 2000), the effective field methods of the Mori–Tanaka type and variational estimates of the Hashin–Shtrikman type, or numerical methods like computational homogenization (CH) (Rungsiyakull et al., 2010; Chen et al., 2013). CH, the most general approach, is preferred in this work.

Then, we proceed to solve the inner problem applying CH over a parameterized Representative Volume Element (RVE). In this way, we build a grid of points (*microparameters vs. homogenized property*) for each one of the independent tensorial components of the physical properties involved in a steady-state thermomechanical problem: the fourth-order elasticity tensor, the second-order thermal expansion tensor, and the second-order thermal conductivity tensor.

After that, recourse is made to the response surface methodology (RSM) in order to fit the grid points for each effective property by a polynomial function of the microparameters. Then, the sensitivity of such property to microstructural changes (i.e., its derivative with respect to the microparameters) is also a polynomial. Let us remark that, using RSM, we do not need either to interpolate a property when the microparameters do not coincide with grid points or to use numerical differentiation. Kamiński (2009) has presented a similar approach to evaluate the sensitivity gradients of the computationally-homogenized properties of random composites. He has considered as microparameter the randomness of the mechanical properties of the microcomponents, and has constructed a response function for each of them.

Regarding the computational cost, let us remind that the seek of the optimal macroscopic response of a structure uses to be a long iterative process. At each iteration, a multiscale problem has to be solved: given the distribution of the microstructure throughout the structure, we obtain the macroscopic distribution of the homogenized properties (solving the inner problem at each sampling point), and then we solve a standard structural problem (the outer problem) to obtain the corresponding macroscopic response. In this work, since the inner problem is solved in an offline way, the outer problem becomes the only online stage, making each iteration as expensive as the solution of a standard problem at the macroscopic scale, i.e., considerably cheaper than the solution of a multiscale problem. This is a major contribution of this paper to the MbD approach.

Further, by accounting for the thermal coupling, this work constitutes a step further in sensitivity analysis of purely mechanical multiscale problems (Fish and Ghouali, 2001; Kamiński, 2014).

Finally, as an example of application, the current technique of sensitivity analysis is applied to determine the effect of microstructural changes on the compliance of a thermally loaded structure made of a bi-material. As result, a considerable improvement of the compliance or the stiffness of the structure can be achieved.

2. The two-scale thermomechanical problem

Let us consider a body $\Omega \subset \mathbb{R}^{\dim}$, Fig. 1, undergoing a steady state thermomechanical loading process: the heat flux q^{wall} and the temperature T^{wall} are prescribed on the boundaries $\partial\Omega_q$ and $\partial\Omega_T$, respectively, while the traction $\mathbf{t}^{\text{wall}}$ and the displacement $\mathbf{u}^{\text{wall}}$ are prescribed on the boundaries $\partial\Omega_\sigma$ and $\partial\Omega_u$, respectively. Considering these boundary conditions, the sets of admissible temperature and displacement fields are

$$\mathcal{T} = \{T(\mathbf{X}) \,|T \in \mathcal{H}^1(\Omega) \text{ and } T = T^{\text{wall}} \text{ on } \partial\Omega_T\}, \tag{1}$$

$$\mathcal{U} = \{\mathbf{u}(\mathbf{X}) \,|\mathbf{u} \in \mathcal{H}^1(\Omega) \text{ and } \mathbf{u} = \mathbf{u}^{\text{wall}} \text{ on } \partial\Omega_u\}, \tag{2}$$

where $\mathcal{H}^1(\Omega)$ is the space of functions having square-integrable first derivatives. The spaces of admissible temperature and displacement variations are

$$\hat{\mathcal{T}} = \{\hat{T}(\mathbf{X}) \,|\hat{T} \in \mathcal{H}^1(\Omega), \text{ and } \hat{T} = 0 \text{ on } \partial\Omega_T\}, \tag{3}$$

$$\hat{\mathcal{U}} = \{\hat{\mathbf{u}}(\mathbf{X}) \,|\hat{u}_i \in \mathcal{H}^1(\Omega), \text{ and } \hat{\mathbf{u}} = \mathbf{0} \text{ on } \partial\Omega_u\}. \tag{4}$$

Then, the current macroscopic thermomechanical problem can be stated in the standard variational format as follows: find $T \in \mathcal{T}$ and $\mathbf{u} \in \mathcal{U}$ satisfying

$$\int_\Omega \mathbf{q}(T) \cdot \nabla_{\mathbf{X}} \widehat{T} \; \mathrm{d}V - \int_{\partial\Omega_q} q^{\text{wall}} \widehat{T} \; \mathrm{d}S = 0, \quad \forall \widehat{T} \in \hat{\mathcal{T}}, \tag{5}$$

$$\int_\Omega \boldsymbol{\sigma}(\mathbf{u}, T) \cdot \nabla^s_{\mathbf{X}} \hat{\mathbf{u}} \; \mathrm{d}V - \int_{\partial\Omega_\sigma} \mathbf{t}^{\text{wall}} \cdot \hat{\mathbf{u}} \; \mathrm{d}S = 0, \quad \forall \hat{\mathbf{u}} \in \hat{\mathcal{U}}, \tag{6}$$

where $\mathbf{q}$ is the macroscopic heat flux vector and $\boldsymbol{\sigma}$ is the macroscopic Cauchy stress tensor. Eq. (5) represents the steady-state heat balance equation in absence of internal heat source, while (6) is the momentum balance equation in absence of body forces and inertial terms.

The problem is completed by the constitutive laws for $\mathbf{q}$ and $\boldsymbol{\sigma}$ at any point $\mathbf{X} \in \Omega$, which are determined in this work from the analysis of the microstructure at this point.

Let the body have a heterogeneous microstructure that, at any point $\mathbf{X} \in \Omega$, is described by a Representative Volume Element (RVE), denoted Ω_μ, shown in Fig. 1. Points in Ω_μ are denoted $\mathbf{y}$. From now on, any quantity $(\cdot)$ described in the domain Ω_μ will be denoted as $(\cdot)_\mu$.

As stated in Appendix A, the macroscopic terms $\mathbf{q}$ and $\boldsymbol{\sigma}$ at $\mathbf{X} \in \Omega$ are defined by the homogenization formulas

$$\mathbf{q} = \frac{1}{|\Omega_\mu|} \int_{\Omega_\mu} \mathbf{q}_\mu \mathrm{d}V_\mu, \tag{7}$$

$$\boldsymbol{\sigma} = \frac{1}{|\Omega_\mu|} \int_{\Omega_\mu} \boldsymbol{\sigma}_\mu \mathrm{d}V_\mu, \tag{8}$$

where $|\Omega_\mu|$ is the volume of Ω_μ.

The constitutive response of the material components at the microscopic level is assumed to be known. Further, for the purpose of this work, the behavior of these microcomponents is assumed to be linear. In such a case, $\mathbf{q}_\mu$ and $\boldsymbol{\sigma}_\mu$ are respectively defined by the Fourier's and Hooke's laws:

$$\mathbf{q}_\mu = -\mathbf{k}_\mu \nabla_{\mathbf{y}} T_\mu, \tag{9}$$

$$\boldsymbol{\sigma}_\mu = \mathbf{C}_\mu \nabla^s_{\mathbf{y}} \mathbf{u}_\mu + \mathbf{d}_\mu \left(T_\mu - T^0\right), \tag{10}$$

where $\mathbf{k}_\mu$ is the thermal conductivity tensor, $\mathbf{C}_\mu$ is the elasticity tensor, $\mathbf{d}_\mu$ is the stress increment per unit temperature, all of them are

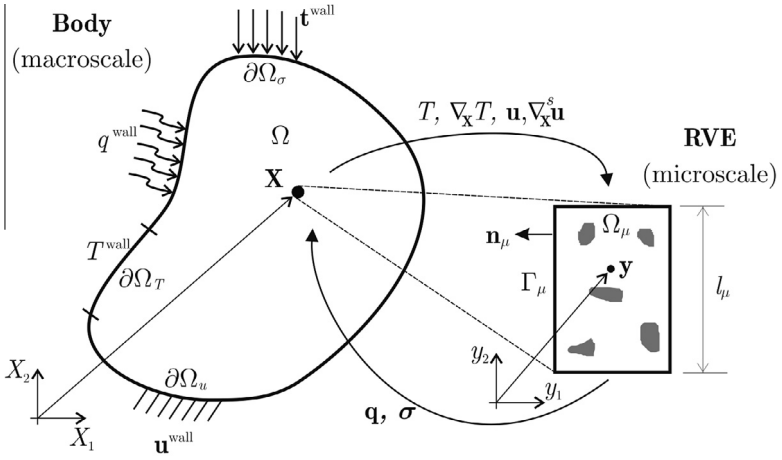

Fig. 1. Two-scale thermomechanical problem.

assumed to be known properties of the material at $\mathbf{y} \in \Omega_\mu$; T^0 is the reference temperature for zero-thermal stress, assumed to be common to all the microcomponents.

For the sake of clarity, the computation of the homogenized fields $\mathbf{q}$ and $\boldsymbol{\sigma}$ is detailed in Appendix A. As shown there, the linearity of the constitutive laws (9) and (10) for the microscopic fields $\mathbf{q}_\mu$ and $\boldsymbol{\sigma}_\mu$ is inherited by the constitutive laws for the homogenized fields $\mathbf{q}$ and $\boldsymbol{\sigma}$, given by

$$\mathbf{q} = -\mathbf{k}\,\nabla_{\mathbf{X}} T, \tag{11}$$

$$\boldsymbol{\sigma} = \mathbf{C}\,\nabla^s_{\mathbf{X}}\mathbf{u} + \mathbf{d}(T - T^0), \tag{12}$$

where we introduce the effective thermal conductivity $\mathbf{k}$, the effective elastic moduli $\mathbf{C}$, and the effective stress increment per unit temperature $\mathbf{d}$, defined by Eqs. (AI-22), (AI-27) and (AI-32) in the Appendix, respectively.

A multiscale mechanical problem accounting for thermal expansion in FGM was studied by Yin et al. (2007). Unlike the current work, they did not use computational homogenization and they did not discuss the sensitivity of the effective material properties to microstructural changes.

3. Finite element model

The thermomechanical problem described in the previous section will be solved using the Finite Element Method (FEM). Let us note that, once the homogenized flux $\mathbf{q}$ and stress $\boldsymbol{\sigma}$ (Eqs. (7) and (8), respectively) are introduced in the heat balance Eq. (5) and the momentum balance Eq. (6), their solution by FEM is completely standard and has been widely discussed in the classic literature (see Zienkiewicz and Taylor, 2000 for instance). For the sake of completeness, it will be summarized in this section.

Using FEM, the unknown temperature and displacement fields are approximated for all $\mathbf{X} \in \Omega$ by

$$T(\mathbf{X}) = \Phi_i(\mathbf{X})T_i = \boldsymbol{\Phi}(\mathbf{X})\mathbf{T}, \tag{13}$$

$$\mathbf{u}(\mathbf{X}) = \Phi_i(\mathbf{X})\mathbf{u}_i = \boldsymbol{\Phi}^{\mathrm{m}}(\mathbf{X})\mathbf{U}, \tag{14}$$

where T_i and $\mathbf{u}_i$ are the temperature and displacement unknowns at the node $\mathbf{X}_i$ ($i = 1, 2, \ldots, \#nodes$) of the finite element mesh, and Φ_i is the shape function associated to this node, such that $\Phi_i(\mathbf{X}_j) = \delta_{ij}$ at any node $\mathbf{X}_j$ of the mesh, δ_{ij} denoting the Kronecker delta; T_i and $\mathbf{u}_i$ are grouped in the column vectors $\mathbf{T}$ and $\mathbf{U}$, respectively, while the shape functions Φ_i are grouped either in the row vector $\boldsymbol{\Phi}$ for thermal analysis or in the matrix $\boldsymbol{\Phi}^{\mathrm{m}}$ for mechanical analysis.

Using standard Galerkin FEM, the shape functions Φ_i also define the basis functions for the finite-dimensional spaces approximating $\hat{\mathcal{T}}$ and $\hat{\mathcal{U}}$. Then, the weak form of the thermal problem (5), after replacing the macroscopic Fourier's law (11), can be written as

$$\mathbf{K}\mathbf{T} = -\mathbf{F}, \tag{15}$$

with

$$\mathbf{K} = \int_\Omega \mathbf{B}^T\mathbf{k}\mathbf{B}\ \mathrm{d}V, \tag{16}$$

$$\mathbf{F} = \int_{\partial\Omega_q} \boldsymbol{\Phi}^T q^{\text{wall}}\mathrm{d}S, \tag{17}$$

where $\mathrm{B}_{ij} = \partial\Phi_i/\partial X_j$ is the matrix of the shape function gradients.

In a similar way, the weak form of the mechanical problem (6), after replacing the constitutive Eq. (12), can be written as

$$\mathbf{K}^{\mathrm{m}}\mathbf{U} = -\mathbf{F}^{\mathrm{tm}}, \tag{18}$$

where

$$\mathbf{K}^{\mathrm{m}} = \int_\Omega (\mathbf{B}^{\mathrm{m}})^T\mathbf{C}\mathbf{B}^{\mathrm{m}}\mathrm{d}V, \tag{19}$$

$$\mathbf{F}^{\mathrm{tm}} = \mathbf{F}^{\mathrm{m}} + \mathbf{F}^{\mathrm{t}}, \tag{20}$$

$$\mathbf{F}^{\mathrm{m}} = \int_{\partial\Omega_\sigma} (\boldsymbol{\Phi}^{\mathrm{m}})^T\mathbf{t}^{\text{wall}}\mathrm{d}S, \tag{21}$$

$$\mathbf{F}^{\mathrm{t}} = -\int_\Omega (\mathbf{B}^{\mathrm{m}})^T\mathbf{d}\left(T - T^0\right)\mathrm{d}V \tag{22}$$

with $\mathbf{B}^{\mathrm{m}}$ denoting the strain–displacement matrix.

4. Sensitivity of the macroscopic thermomechanical response to microstructural changes

For the sake of generality, let the microstructure vary throughout the macroscopic domain Ω. Using FEM, Ω is represented by a mesh of finite elements, giving rise to a finite number of sampling points $\mathbf{X}_\alpha$. Each point $\mathbf{X}_\alpha$ has an associated RVE denoted $\Omega^{(\alpha)}_\mu$.

Let us remind that we deal with "quantitatively characterized materials" (Kachanov and Sevostianov, 2005), those where the microstructure at any RVE $\Omega^{(\alpha)}_\mu$ can be described by a finite (usually reduced) number of parameters $p^{(\alpha)}_1, p^{(\alpha)}_2, \ldots$. These are the so-called microstructural parameters or, simply, microparameters. Examples

of microparameters are the fiber orientation in fiber-reinforced polymers (Lund and Stegmann, 2005), the porosity and the eccentricity in solids with elliptic holes (Kachanov and Sevostianov, 2005), the size and the volume fraction of particles in dental coating (Rungsiyakull et al., 2010), etc.

For such materials, any effective property at a point $\mathbf{X}_\alpha \in \Omega$ is ultimately a function of the parameters $p_1^{(\alpha)}, p_2^{(\alpha)}, \ldots$ corresponding to the RVE at $\mathbf{X}_\alpha$; for instance, the effective conductivity at $\mathbf{X}_\alpha$ is $\mathbf{k}(\mathbf{X}_\alpha) = \mathbf{k}(p_1^{(\alpha)}, p_2^{(\alpha)}, \ldots)$. Considering that the macroscopic response of the whole body is made of contributions from all the sampling points $\mathbf{X}_1, \mathbf{X}_2, \ldots$ of the finite element mesh, the macroscopic fields T and $\mathbf{u}$ depend on all the microparameters defining the RVEs at all these points, i.e. $T = T(\mathbf{P})$ and $\mathbf{u} = \mathbf{u}(\mathbf{P})$, with

$$\mathbf{P} = \left[p_1^{(1)}, p_2^{(2)}, \ldots p_1^{(2)}, p_2^{(2)}, \ldots\right]. \tag{23}$$

The thermomechanical macroscopic response is defined by a given function $\mathcal{R}$, the so-called objective or cost function in structural optimization problems (Bendsøe and Sigmund, 2003), which depends on global nodal temperature and displacement vectors as primal variables, i.e.

$$\mathcal{R} = \mathcal{R}(\mathbf{U}, \mathbf{T}), \tag{24}$$

where $\mathbf{U}$ and $\mathbf{T}$ satisfy their respective balance Eqs. (15) and (18). Hence, the balance equations are implicit in the objective function $\mathcal{R}$, that is, they are not regarded as constraints in the current sensitivity analysis. This approach is favored by the linearity of the balance equations (15) and (18).

The sensitivity of the macroscopic response (24) to a change in the microparameter P_i is

$$\frac{\mathrm{d}\mathcal{R}}{\mathrm{d}P_i} = \frac{\partial \mathcal{R}}{\partial U_j}\frac{\partial U_j}{\partial P_i} + \frac{\partial \mathcal{R}}{\partial T_j}\frac{\partial T_j}{\partial P_i}, \tag{25}$$

where $(\cdot)_j$ denotes the jth entry of the vector $(\cdot)$.

The computation of the sensitivity of $\mathbf{T}$ and $\mathbf{U}$ to microstructural changes is the goal of Sections 4.1 and 4.2, respectively.

4.1. Sensitivity of the macroscopic temperature to microstructural changes

Since the effective thermal conductivity tensor $\mathbf{k}$ depends on the parameterized microstructure according to Eq. (AI-22), a variation $\delta\mathbf{P}$ of the microstructure induces the following variation in the conductivity matrix (Eq. (16)):

$$\delta\mathbf{K} = \int_\Omega \mathbf{B}^T \delta\mathbf{k}\mathbf{B}\ \mathrm{d}V. \tag{26}$$

The variations of (any nonsingular matrix) $\mathbf{K}$ and its inverse are related by

$$\delta\left(\mathbf{K}^{-1}\right) = -\mathbf{K}^{-1}\delta\mathbf{K}\ \mathbf{K}^{-1}. \tag{27}$$

Then, the variation of the nodal temperature vector $\mathbf{T}$, solution of the linear heat balance Eq. (15), can be expressed as

$$\delta\mathbf{T} = \delta\left(\mathbf{K}^{-1}\right)\mathbf{F} = -\mathbf{K}^{-1}\delta\mathbf{K}\ \mathbf{K}^{-1}\mathbf{F} = -\mathbf{K}^{-1}\delta\mathbf{K}\mathbf{T}. \tag{28}$$

Therefore, the sensitivity of the nodal temperature vector $\mathbf{T}$ to a change in P_i is

$$\frac{\partial \mathbf{T}}{\partial P_i} = -\mathbf{K}^{-1}\mathbf{s}_i, \tag{29}$$

where $\mathbf{s}_i$ is the column vector

$$\mathbf{s}_i = \frac{\partial \mathbf{K}}{\partial P_i}\mathbf{T} \tag{30}$$

and the derivative of $\mathbf{K}$, obtained by differentiation of Eq. (26), is

$$\frac{\partial \mathbf{K}}{\partial P_i} = \int_\Omega \mathbf{B}^T \frac{\partial \mathbf{k}}{\partial P_i}\mathbf{B}\ \mathrm{d}V. \tag{31}$$

Now, the sensitivity of the macroscopic temperature field (given in FEM form by Eq. (13)) to a change of P_i is

$$\frac{\partial \mathbf{T}}{\partial P_i} = -\mathbf{\Phi}\mathbf{K}^{-1}\mathbf{s}_i, \tag{32}$$

which, evaluated at the node $\mathbf{X}_j$, takes the form

$$\frac{\partial T_j}{\partial P_i} = -\mathbf{j}\cdot\mathbf{s}_i, \tag{33}$$

where $\mathbf{j}$ refers to the jth row of $\mathbf{K}^{-1}$. Let us note that $\partial T_j/\partial P_i$ is generally non null for any node $\mathbf{X}_j \notin \partial\Omega_T$, even if P_i describes the microstructure at a point far from the node $\mathbf{X}_j$. This non-local effect of microstructural changes is detrimental to the computational cost of sensitivity analysis in thermomechanical problems, as it will be realized in Section 4.2.1. Let us note that this effect is disregarded if the thermal expansion is assumed to be homogeneous throughout the macroscopic body (as done by Bendsøe and Sigmund, 2003). To the authors' opinion, this is generally an excessively restrictive hypothesis.

4.1.1. FEM implementation details

If P_i (totally or partially) defines the microstructure at a sampling point $\mathbf{X}_\alpha$ inside a given finite element Ω^e, then $\partial\mathbf{k}/\partial P_j = 0$ at $\mathbf{X}_\alpha$ when P_j is associated to any other sampling point. Therefore, only the sampling point $\mathbf{X}_\alpha \in \Omega^e$ contributes to the global matrix $\partial\mathbf{K}/\partial P_i$, Eq. (31), i.e.:

$$\frac{\partial \mathbf{K}}{\partial P_i} = \left[\mathbf{B}^T\frac{\partial \mathbf{k}}{\partial P_i}\mathbf{B}\right]_{\mathbf{X}_\alpha} w_\alpha \quad \text{(no summation over } \alpha\text{)}, \tag{34}$$

where w_α is the weight associated to the sampling point $\mathbf{X}_\alpha \in \Omega^e$. Therefore, $\partial\mathbf{K}/\partial P_i$ is markedly sparse and can be computed based on only one element, and these properties are inherited by the global vector $\mathbf{s}_i$ given by Eq. (30).

4.2. Sensitivity of the macroscopic displacement to microstructural changes

In Eq. (19) defining the stiffness matrix $\mathbf{K}^{\mathrm{m}}$, the elasticity tensor $\mathbf{C}$ depends on the parameterized microstructure. Then, a variation $\delta\mathbf{P}$ induces the following variation in the stiffness matrix:

$$\delta\mathbf{K}^{\mathrm{m}} = \int_\Omega \left(\mathbf{B}^{\mathrm{m}}\right)^T \delta\mathbf{C}\mathbf{B}^{\mathrm{m}}\mathrm{d}V. \tag{35}$$

On the other hand, in the definition of the nodal load vector $\mathbf{F}^{\mathrm{tm}}$ (Eq. (20)), only the thermal-stress contribution $\mathbf{F}^{\mathrm{t}}$ (Eq. (22)) depends on microstructure through the effective property $\mathbf{d}$ and the macroscopic temperature field T. Thus, a variation $\delta\mathbf{P}$ produces the variation

$$\delta\mathbf{F}^{\mathrm{tm}} \equiv \delta\mathbf{F}^{\mathrm{t}} = -\int_\Omega \left(\mathbf{B}^{\mathrm{m}}\right)^T \delta\mathbf{d}\left(T - T^0\right)\mathrm{d}V - \int_\Omega \left(\mathbf{B}^{\mathrm{m}}\right)^T \mathbf{d}\,\delta T\,\mathrm{d}V. \tag{36}$$

Then, the variation of the nodal displacement vector $\mathbf{U}$ (solution of the linear equilibrium equation (18)) is

$$\begin{aligned}\delta\mathbf{U} &= \delta\left[\left(\mathbf{K}^{\mathrm{m}}\right)^{-1}\right]\mathbf{F}^{\mathrm{tm}} + \left(\mathbf{K}^{\mathrm{m}}\right)^{-1}\delta\mathbf{F}^{\mathrm{tm}} = -\left(\mathbf{K}^{\mathrm{m}}\right)^{-1}\left[\delta\mathbf{K}^{\mathrm{m}}\left(\mathbf{K}^{\mathrm{m}}\right)^{-1}\mathbf{F}^{\mathrm{tm}} - \delta\mathbf{F}^{\mathrm{tm}}\right] \\ &= -\left(\mathbf{K}^{\mathrm{m}}\right)^{-1}\left(\delta\mathbf{K}^{\mathrm{m}}\mathbf{U} - \delta\mathbf{F}^{\mathrm{tm}}\right),\end{aligned} \tag{37}$$

from which it can be derived that the sensitivity of the global nodal displacement vector $\mathbf{U}$ to a change in the microparameter P_i is

$$\frac{\partial \mathbf{U}}{\partial P_i} = -\left(\mathbf{K}^{\mathrm{m}}\right)^{-1}\mathbf{s}_i^{\mathrm{m}}, \tag{38}$$

where $\mathbf{s}_i^{\mathrm{m}}$ is the column vector

$$\mathbf{s}_i^{\mathrm{m}} = \frac{\partial \mathbf{K}^{\mathrm{m}}}{\partial P_i}\mathbf{U} - \frac{\partial \mathbf{F}^{\mathrm{tm}}}{\partial P_i} \tag{39}$$

with

$$\frac{\partial \mathbf{K}^{\mathrm{m}}}{\partial P_i} = \int_\Omega \left(\mathbf{B}^{\mathrm{m}}\right)^T \frac{\partial \mathbf{C}}{\partial P_i}\mathbf{B}^{\mathrm{m}}\mathrm{d}V, \tag{40}$$

$$\frac{\partial \mathbf{F}^{\mathrm{tm}}}{\partial P_i} = \left.\frac{\partial \mathbf{F}^{\mathrm{tm}}}{\partial P_i}\right|_{T=constant} + \left.\frac{\partial \mathbf{F}^{\mathrm{tm}}}{\partial P_i}\right|_{\mathbf{d}=constant}, \tag{41}$$

$$\left.\frac{\partial \mathbf{F}^{\mathrm{tm}}}{\partial P_i}\right|_{T=constant} \equiv \left.\frac{\partial \mathbf{F}^{\mathrm{t}}}{\partial P_i}\right|_{T=constant} = -\int_\Omega \left(\mathbf{B}^{\mathrm{m}}\right)^T \frac{\partial \mathbf{d}}{\partial P_i}\left(T - T^0\right)\mathrm{d}V, \tag{42}$$

$$\left.\frac{\partial \mathbf{F}^{\mathrm{tm}}}{\partial P_i}\right|_{\mathbf{d}=constant} \equiv \left.\frac{\partial \mathbf{F}^{\mathrm{t}}}{\partial P_i}\right|_{\mathbf{d}=constant} = -\int_\Omega \left(\mathbf{B}^{\mathrm{m}}\right)^T \mathbf{d}\,\frac{\partial T}{\partial P_i}\mathrm{d}V. \tag{43}$$

4.2.1. FEM implementation details

Like in Section 4.1.1, if the microparameter P_i is associated to a sampling point $\mathbf{X}_\alpha$ inside a given finite element Ω^e, only this sampling point contributes to the global matrix $\partial\mathbf{K}^{\mathrm{m}}/\partial P_i$ (Eq. (40)), that is

$$\frac{\partial \mathbf{K}^{\mathrm{m}}}{\partial P_i} = \left[\left(\mathbf{B}^{\mathrm{m}}\right)^T \frac{\partial \mathbf{C}}{\partial P_i}\mathbf{B}^{\mathrm{m}}\right]_{\mathbf{X}_\alpha} w_\alpha \quad \text{(no summation over } \alpha\text{)}. \tag{44}$$

Similarly, the global vector (42) is built by the contribution of only this sampling point, i.e.

$$\left.\frac{\partial \mathbf{F}^{\mathrm{tm}}}{\partial P_i}\right|_{T=constant} = -\left[\left(\mathbf{B}^{\mathrm{m}}\right)^T \frac{\partial \mathbf{d}}{\partial P_i}\left(T - T^0\right)\right]_{\mathbf{X}_\alpha} w_\alpha \quad \text{(no summation over } \alpha\text{)}. \tag{45}$$

However, this is not the case for the global vector (43) since its integrand has the factor

$$\left[\frac{\partial T}{\partial P_j}\right]_{\mathbf{X}_\beta} = -\mathbf{\Phi}(\mathbf{X}_\beta)\mathbf{K}^{-1}\mathbf{s}_j, \tag{46}$$

which is generally non null for any microparameter P_j and for any sampling point $\mathbf{X}_\beta \notin \partial\Omega_T$, even if P_j describes the microstructure at a point far from $\mathbf{X}_\beta$, as discussed after Eq. (33). Hence, the global vector $\partial\mathbf{F}^{\mathrm{tm}}/\partial P_i|_{\mathbf{d}=constant}$ must be built by assembling the contributions of all the finite elements of the mesh, and it is not sparse. Therefore, when the thermal expansion is sensitive to microstructural changes, the computation of the sensitivity of the macroscopic mechanical response requires considerably more computational resources (memory to store all the non-sparse vectors $\partial\mathbf{F}^{\mathrm{tm}}/\partial P_i|_{\mathbf{d}=constant}$, and time for solving the operations involving these non-sparse vectors) than the case where the thermal expansion is fixed (see Bendsøe and Sigmund, 2003).

5. Offline computation of the effective properties and their sensitivities

The microstructure of the materials addressed in the current paper are assumed to be adequately characterized by a few number of parameters $p_1, p_2, \ldots, p_n$. Then, we propose to use an offline strategy based on the response surface methodology (RSM). This strategy circumvents the solution of the microscopic problem of determining the effective properties during the online solution of the macroscopic problem. In this way, the time needed to compute the macroscopic response (24) for variable microstructure is hugely reduced.

Let f be a scalar component of an effective material property, either k_{ij}, C_{ijkl} or d_{ij} as defined by Eqs. (AI-22), (AI-27) and (AI-32), respectively. First, we compute f for a n-dimensional grid of predefined points $(p_1^{\mathrm{g}}, p_2^{\mathrm{g}}, \ldots, p_n^{\mathrm{g}})$. Once the grid for f is built, the values of f for intermediate points $(p_1, p_2, \ldots, p_n)$ can be computed by interpolation and the sensitivity $\partial f/\partial p_i$ can be computed by numerical differentiation.

For the purpose of convenience, the grid data is used in this paper to build a closed-form response surface function $\tilde{f}$ to approximate f. The procedure is illustrated in Fig. 2: at a point $\mathbf{X}_\alpha \in \Omega$, where the microstructure is characterized by the parameters $(p_1^{(\alpha)}, p_2^{(\alpha)}, \ldots p_n^{(\alpha)})$, the value of the effective property f is assumed to be $f(\mathbf{X}_\alpha) \equiv \tilde{f}(p_1^{(\alpha)}, p_2^{(\alpha)}, \ldots p_n^{(\alpha)})$. Consequently, the sensitivity of f to a change in the microparameter $p_i^{(\alpha)}$ is the closed-form function $\partial\tilde{f}/p_i^{(\alpha)}$. This procedure is detailed for a particular microstructure in Section 6.1.

Finally, let us note that some authors (Rungsiyakull et al., 2010; Chen et al., 2013; Hou et al., 2008) use the RSM to approximate the macroscopic response of the body rather than the effective properties. Such strategy is discouraged for the design of a body with heterogeneous microstructure, since its response depends generally on so many variables (the whole set of microparameters) that RSM becomes unaffordable.

6. Application

Let us consider the cantilever plate depicted in Fig. 3(a), deformed by keeping its top surface at temperature T^{top} and its bottom surface at temperature $T^{\mathrm{bottom}} < T^{\mathrm{top}}$.

For the sake of simplicity, the plate is assumed to be under plane strain conditions. The macroscopic domain Ω is the rectangle $B \times H$ representing a slice of unit width of the whole plate, parallel to the plane X_1–X_2. We adopt the same finite element mesh to represent Ω for thermal and mechanical analysis. We use standard Q1 finite elements, which have a quadrangular geometry, four nodes located at the vertices and bilinear shape functions. The whole macroscopic mesh contains 80×20 Q1 finite elements of constant size $\Delta X_1 \times \Delta X_2$. All the parameters defining the macroscopic problem are listed in Table 1.

The plate is made of a composite, which is manufactured with two materials, say $\mathrm{M}^{\mathrm{layer}}$ and $\mathrm{M}^{\mathrm{matrix}}$, arranged according to Fig. 3(b). Horizontal and vertical layers of $\mathrm{M}^{\mathrm{layer}}$ are sandwiched using the support material $\mathrm{M}^{\mathrm{matrix}}$. The distance between two successive vertical or horizontal layers is $l_\mu = constant$, with $l_\mu \ll H$.

Let us allow the microstructure to change from node to node throughout Ω. Then, every node $\mathbf{X}_\alpha \in \Omega$ has its own microstructure and, consequently, its associated RVE, say $\Omega_\mu^{(\alpha)}$. Due to the nearly periodic microstructure, $\Omega_\mu^{(\alpha)}$ can be taken as a square cell of side $l_\mu = constant$, subjected to periodic boundary conditions, as shown in Fig. 3(c). This RVE is made of $\mathrm{M}^{\mathrm{matrix}}$ as support material, crossed by one vertically centered layer of thickness b_α and one horizontal centered layer of thickness h_α of material $\mathrm{M}^{\mathrm{layer}}$. Let us assume that the materials $\mathrm{M}^{\mathrm{matrix}}$ and $\mathrm{M}^{\mathrm{layer}}$ are given. Therefore, the RVE at $\mathbf{X}_\alpha$ is completely defined by two microparameters: $p_1^{(\alpha)} = b_\alpha$ and $p_2^{(\alpha)} = h_\alpha$.

Both materials $\mathrm{M}^{\mathrm{matrix}}$ and $\mathrm{M}^{\mathrm{layer}}$ are assumed to be isotropic and to obey the Fourier's heat flow law (9) and the linear thermoelastic law (10). The mechanical properties at a point $\mathbf{y} \in \Omega_\mu^{(\alpha)}$ are

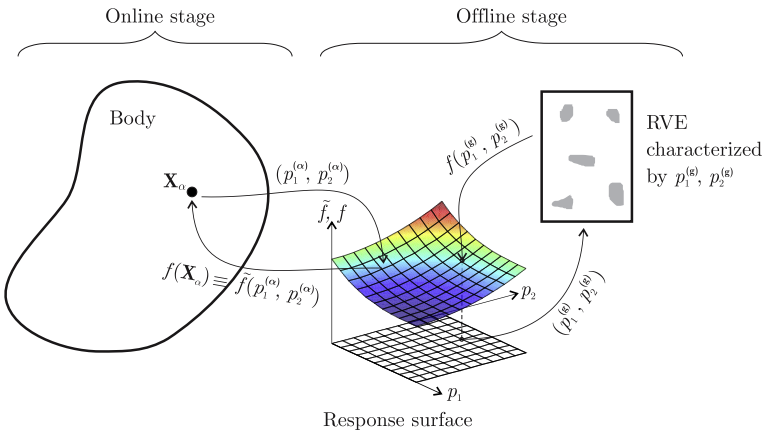

Fig. 2. Offline computation of the response surface $\tilde{f}$ for the effective property f. The effective property is given hereafter by the response surface function $\tilde{f}$ for the online computation of the macroscopic thermomechanical response.

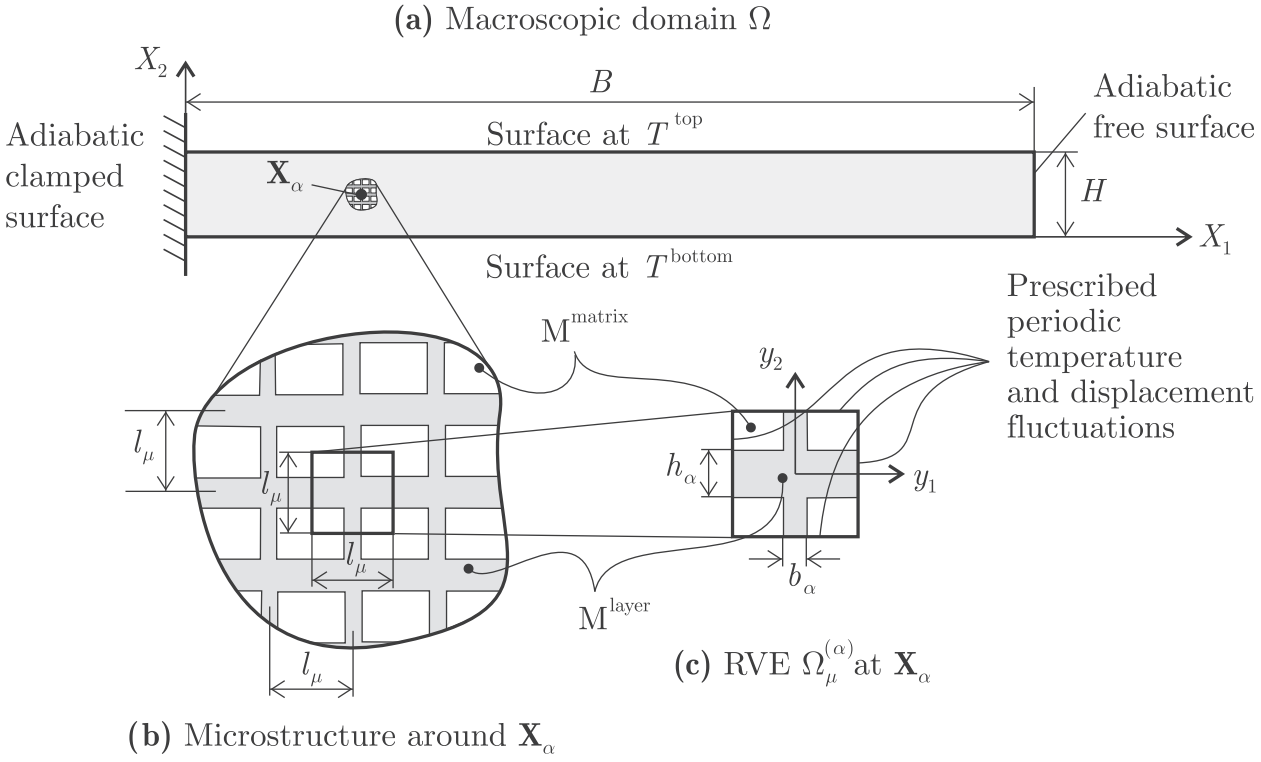

Fig. 3. Multiscale analysis of a cantilever plate: (a) macroscopic domain Ω with thermal and mechanical boundary conditions, (b) microstructure around the point $\mathbf{X}_\alpha \in \Omega$, (c) RVE $\Omega_\mu^{(\alpha)}$ at the point $\mathbf{X}_\alpha \in \Omega$, with periodic boundary conditions.

Table 1
Parameters for the macroscopic problem.

B	3 m
H	0.3 m
ΔX_1	3.75 cm
ΔX_2	1.5 cm
T^{top}	50 °C
T^{bottom}	0 °C

$$C_{\mu_{ijkl}} = \frac{Ev}{(1+v)(1-2v)}\delta_{ij}\delta_{kl} + \frac{E}{2(1+v)}\left(\delta_{ik}\delta_{jl} + \delta_{il}\delta_{jk}\right), \tag{47}$$

$$d_{\mu_{ij}} = -\frac{E}{1-2v}\alpha\delta_{ij}, \tag{48}$$

Table 2
Material properties.

Property	M^{matrix} (steel)	M^{layer} (copper)
Young's modulus	200 GPa	120 GPa
Poisson ratio	0.30	0.34
Linear thermal expansion coefficient	1.0×10^{-5}/°C	1.7×10^{-5}/°C
Thermal conductivity	36.5 W/(m °C)	384.0 W/(m °C)

where E is the Young's modulus, v is the Poisson ratio and α is the linear thermal expansion coefficient, all of them are known properties of the material at $\mathbf{y}$ (either M^{matrix} or M^{layer}). In this example, we adopt steel as M^{matrix} and copper as M^{layer}, whose properties are listed in Table 2. The reason for this choice lies in the considerable difference between the thermomechanical properties of such

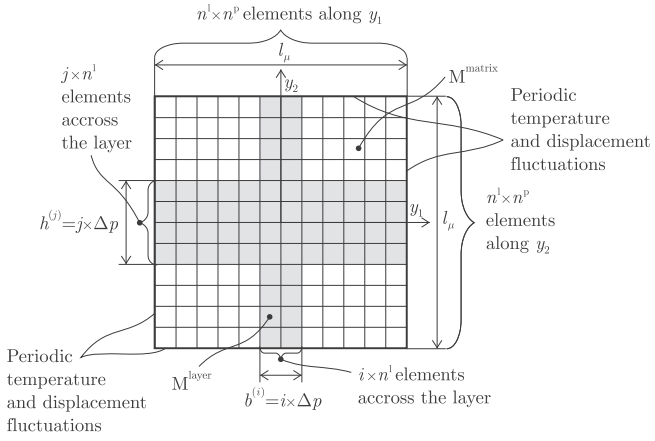

Fig. 4. Finite element model of the RVE used for the offline homogenization of the material properties.

materials, emphasizing the influence of microstructural parameters on the macroscopic response.

6.1. Offline homogenization of the thermomechanical properties

For the homogenization of the material properties, we define a generic RVE, Ω_μ, geometrically equal to a square of side l_μ, subject to periodic boundary conditions in temperature and displacement fluctuations, as shown in Fig. 4. This RVE has M^{matrix} as support material, a vertical layer of variable thickness b and a horizontal layer of variable thickness h, being M^{layer} the material in the layers.

In order to obtain adequately accurate solutions, it is convenient to make each layer in the RVE at least one-element thick, which is unfeasible when the thickness of the layer is too small but positive. In this paper, this is circumvented by choosing b and h from the discrete sets $\{0, b^{(1)}, b^{(2)}, \ldots, b^{(n^p)}\}$ and $\{0, h^{(1)}, h^{(2)}, \ldots, h^{(n^p)}\}$, where $b^{(i)} = h^{(i)} = i\Delta p$, $b^{(n^p)} = h^{(n^p)} = l$, and n^p is a large-enough integer.

Table 3
Parameters for the microscale problem.

l_μ	1 cm
n^l	2
n^p	50
Δy	0.01 cm
Δp	0.02 cm

Then, a unique mesh is used to represent the RVE resulting from any pair $\{b^{(i)}, h^{(j)}\}$. This is a rectangular mesh of Q_1 square finite elements of side $\Delta y = l_\mu/(n^l n^p)$, with $n^l = 2, 4, \ldots$. In this way, there are n^l elements across the layer at the worst case (when the thickness of one of the layers is equal to Δp and the thickness of the other layer is less than l_μ), as shown in Fig. 4. Table 3 lists all the parameters adopted here to define the current RVE.

By the way, if the sampling points of Q_1 elements are located – as usual – strictly inside the elements, this approach eliminates the ambiguity when defining the material at sampling points, since they never lie on a material interface.

For each point $\{b^{(i)}, h^{(j)}\}$ of the grid, we build the corresponding RVE with a $b^{(i)}$-thick vertical layer and a $h^{(j)}$-thick horizontal layer of material M^{layer}. We use this RVE to compute the effective material properties $\mathbf{k}(b^{(i)}, h^{(j)})$ using Eq. (AI-22), $\mathbf{C}(b^{(i)}, h^{(j)})$ using Eq. (AI-27) and $\mathbf{d}(b^{(i)}, h^{(j)})$ using Eq. (AI-32). This produces a set of $(n^p + 1)^2$ triplets $\{b, h, f(b, h)\}$, one set for each independent component of the tensors $\mathbf{k}, \mathbf{C}$ and $\mathbf{d}$. Fig. 5 shows the so-computed grids for $f \equiv k_{11}$, $f \equiv C_{1111}$ and $f \equiv d_{11}$ respectively.

6.1.1. Validation of the macroscopic analysis with offline-homogenized properties

For the purpose of validation of the current strategy, let us solve the problem of the thermally-loaded composite cantilever plate shown in Fig. 3 using direct numerical simulation (DNS). In this case, the finite element mesh of the macroscopic domain Ω is fine-enough to capture the microscale morphology, avoiding in such a way the need of homogenizing the material properties.

A large set of tests were run for the plate made of different composites. In any case, the composite has M^{matrix} as support material, and either vertical, horizontal or crossed layers (two layers of equal thickness, one vertical and one horizontal) of M^{layer}; the thickness of the layers changes from test to test. Then, all the tests were solved using DNS as well as the current multiscale strategy with offline-homogenized effective properties. The DNS mesh has 225000 Q1 finite elements, while the mesh for the current strategy has 1600 Q1 elements.

Fig. 6 shows the magnitude of the maximum deflection of the plate, v^{tip}, which occurs at the right lower edge. As seen there, the results obtained using both methods are in very good agreement.

The major difference between DNS and the current proposal lies in their computational demands. Both methods were implemented in the MatLab® environment using its vectorization capability, and all the tests were run employing an Intel® Core™ i7-3770K CPU. The average time for a DNS run was 152.2 s, while the average time for a run using the current strategy was 0.2 s. This enormous saving

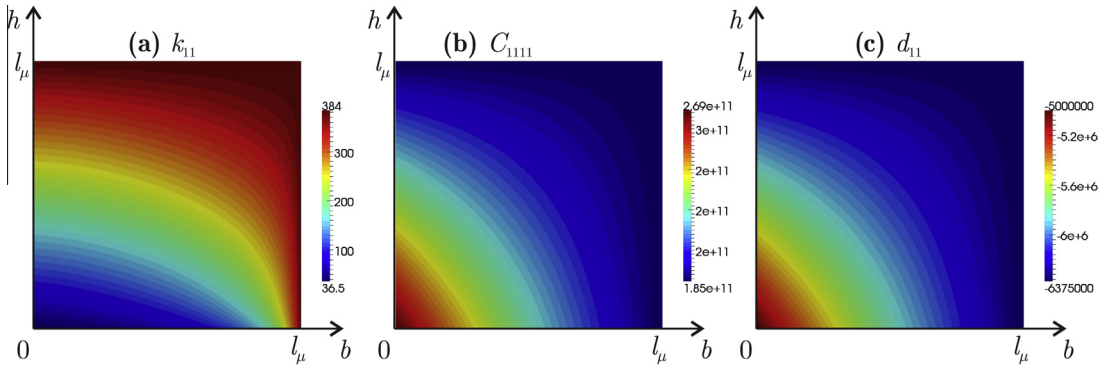

Fig. 5. Grids for effective properties as functions of b and h ($0 \leqslant b,\ h \leqslant l_\mu$): (a) k_{11} in (W/(m °C)) computed using Eq. (AI-22); (b) C_{1111} in (Pa) computed using Eq. (AI-27); (c) d_{11} in (Pa/°C) computed using Eq. (AI-32).

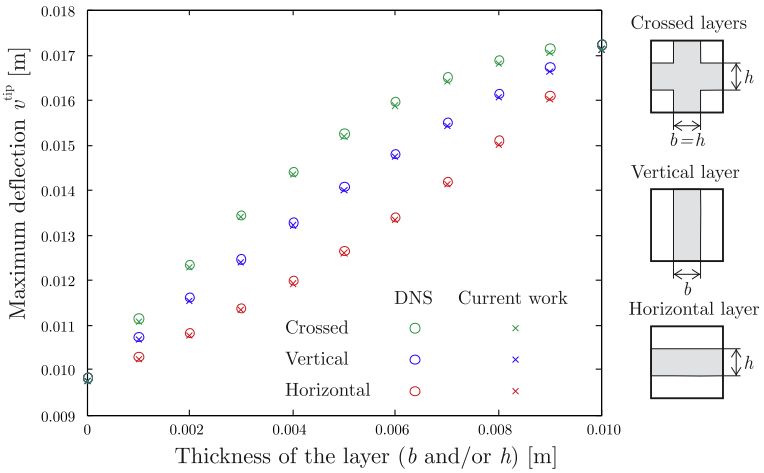

Fig. 6. Maximum deflection of the thermally-loaded plate, as computed using direct numerical simulation (DNS) and the current multiscale model.

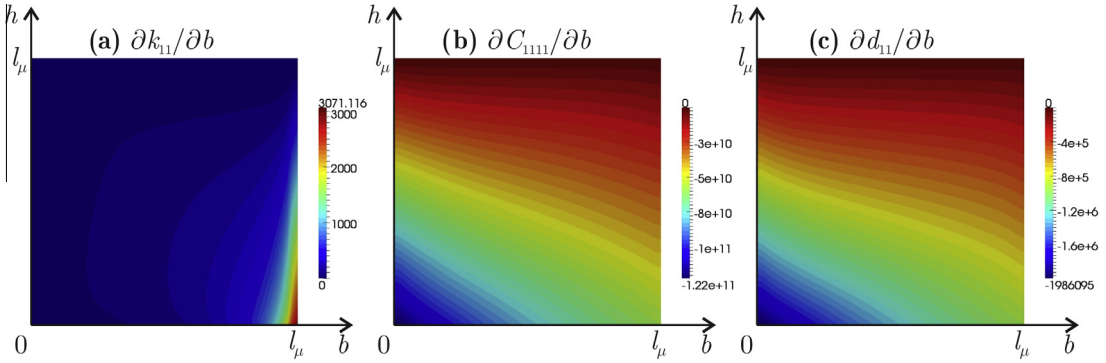

Fig. 7. Derivatives of effective properties as functions of b and h ($0 \leqslant b,\ h \leqslant l_\mu$), numerically computed using the grids in Fig. 5: (a) $\partial k_{11}/\partial b$ in (W/(m^2 °C)); (b) $\partial C_{1111}/\partial b$ in (Pa/m); (c) $\partial d_{11}/\partial b$ in (Pa/(m°C)).

in computational time opens the way to sophisticated industrial applications of the Material by Design approach.

6.2. Response surfaces for the effective properties

Once the grid for a generic effective property f is built, as explained in Section 6.1, the value of f at intermediate values of b and h can be computed using interpolation methods. At the same time, the derivatives of f with respect to b or h can be computed using numerical differentiation techniques. For instance, let us compute the derivatives in the interior points of the grid using central differences, and the derivatives in the boundary points using either backward or forward differences. The so-computed numerical derivatives $\partial k_{11}/\partial b$, $\partial C_{1111}/\partial b$ and $\partial d_{11}/\partial b$ are shown in Fig. 7.

Once $\partial f/\partial b$ and $\partial f/\partial h$ are computed using numerical differentiation at all the grid points, the derivatives $\partial f/\partial b$ and $\partial f/\partial h$ at intermediate points of the grid can be determined by interpolation. For instance, let f and its derivatives be computed for intermediate points using linear interpolation. In such a case, the interpolated derivatives of f are not the derivatives of the interpolated f, which is actually discontinuous at the grid points.

In order to avoid this, let us approximate f using a smooth-enough, closed-form function $\tilde{f}(b,h)$ (the *response surface*) defined for real values of b and h between 0 and l_μ. A simple choice for $\tilde{f}$ is the polynomial function:

$$\tilde{f}(b,h) = \sum_{n=0}^{N}\sum_{m=0}^{N} a_{nm} b^n h^m. \tag{49}$$

The coefficients a_{nm} are computed such that $\tilde{f}$ be the least-squares best approximation to all the points of the f-grid for different values of N. Polynomial of different degrees are necessary in order to approximate different material properties. This approach is similar to that of Kamiński (2009), who proposed a one-dimensional polynomial as response function for the elastic moduli.

Fig. 8(d)–(i) shows the response surfaces for C_{1111}, k_{11} and d_{11} using different polynomial degrees N (their respective grids depicted in Fig. 8(a)–(c), which have already been shown in Fig. 5, are included for comparison purposes). The agreement of the polynomial fitting is measured by the relative error

$$e_i = \left|\frac{f_i - \tilde{f}_i}{f_i}\right|, \tag{50}$$

where the subscript i identifies any point of the f-grid. The maximum values of e_i for those non-zero effective properties and for different polynomial degrees N are listed in Table 4. Although such errors are acceptably small for lower values of N, we finally adopt the largest N listed in Table 4, a choice that will be justified in Section 6.3.

6.3. Computation of the sensitivity of effective properties using the response surfaces

Once a generic effective property f is approximated by the polynomial (response surface) function $\tilde{f}$, Eq. (49), the sensitivity of this effective property to changes in the microstructure parameters is given by the polynomials

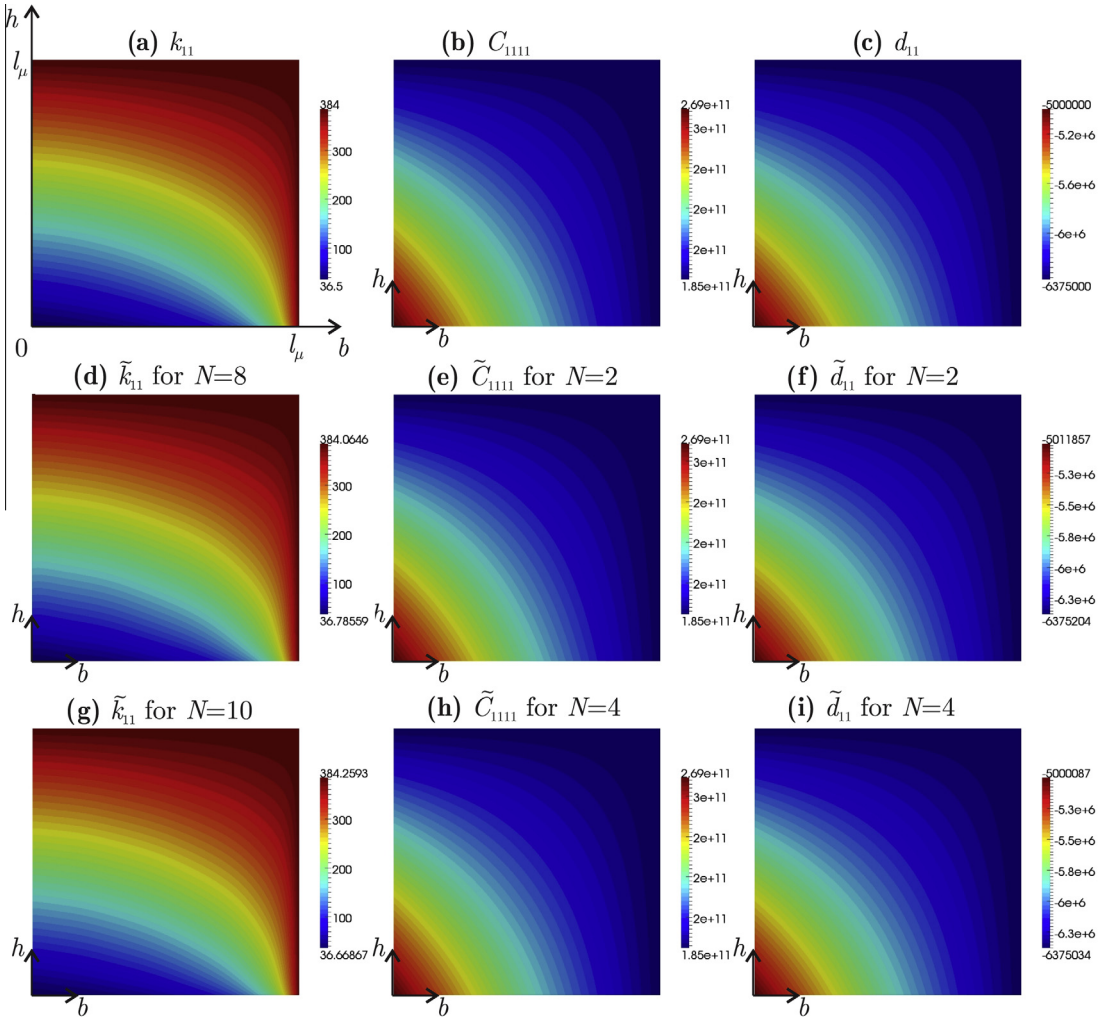

Fig. 8. Effective properties as functions of b and h ($0 \leqslant b,\ h \leqslant l_\mu$): (a)–(c) grids for k_{11} (in (W/(m °C))), C_{1111} (in (Pa)) and d_{11} (in (Pa/°C)), respectively, already depicted in Fig. 5; (d)–(i) response surfaces approximating these properties for different polynomial degrees N.

Table 4
Maximum relative error e_i for different degrees N of polynomial approximations to the tensorial non-zero components of the effective material properties.

Effective property	N	max(e_i) (%)	N	max(e_i) (%)
k_{11}	4	24.52	8	1.78
	6	6.82	10	0.58
k_{22}	4	24.52	8	2.06
	6	6.83	10	1.61
C_{1111}	1	2.40	3	0.11
	2	0.25	4	0.03
C_{1122}	1	1.93	3	0.08
	2	0.22	4	0.03
C_{2222}	1	2.40	3	0.11
	2	0.25	4	0.03
C_{3333}	1	6.98	3	0.15
	2	1.16	4	0.04
d_{11}	1	2.11	3	0.04
	2	0.24	4	0.01
d_{22}	1	2.11	3	0.04
	2	0.24	4	0.01

$$\frac{\partial \tilde{f}(b,h)}{\partial b} = \sum_{n=1}^{N}\sum_{m=0}^{N} n a_{nm} b^{n-1} h^m, \tag{51}$$

$$\frac{\partial \tilde{f}(b,h)}{\partial h} = \sum_{n=0}^{N}\sum_{m=1}^{N} m a_{nm} b^{n} h^{m-1}. \tag{52}$$

Fig. 9(d)–(i) shows the so-computed derivatives $\partial\tilde{k}_{11}/\partial b$, $\partial\tilde{C}_{1111}/\partial b$ and $\partial\tilde{d}_{11}/\partial b$, for two values of N (once again, Fig. 9(a)–(c) are identical to those already depicted in Fig. 7, but are included in Fig. 9 for the purpose of comparison). Taking the grid of numerical derivatives as reference, it is apparent from Fig. 9 that only the polynomial approximations having the highest degree in Table 4 provide qualitative and quantitatively acceptable results when their derivatives are considered.

6.4. Sensitivity of the macroscopic response to microstructural changes

A common choice to characterize the macroscopic response $\mathcal{R}$ of a structure, widely used in purely mechanical problems (Bendsøe and Sigmund, 2003), is the total work performed by the external loads:

$$\mathcal{R} = \mathbf{U}^T\mathbf{K}\mathbf{U} = \mathbf{U}^T\mathbf{F}^{\mathrm{tm}}. \tag{53}$$

For given external loads, to minimize $\mathcal{R}$ implies to maximize the stiffness of the whole structure. Respectively, to maximize $\mathcal{R}$ implies to maximize the compliance of the structure. The sensitivity of the response (53) to microstructural changes is

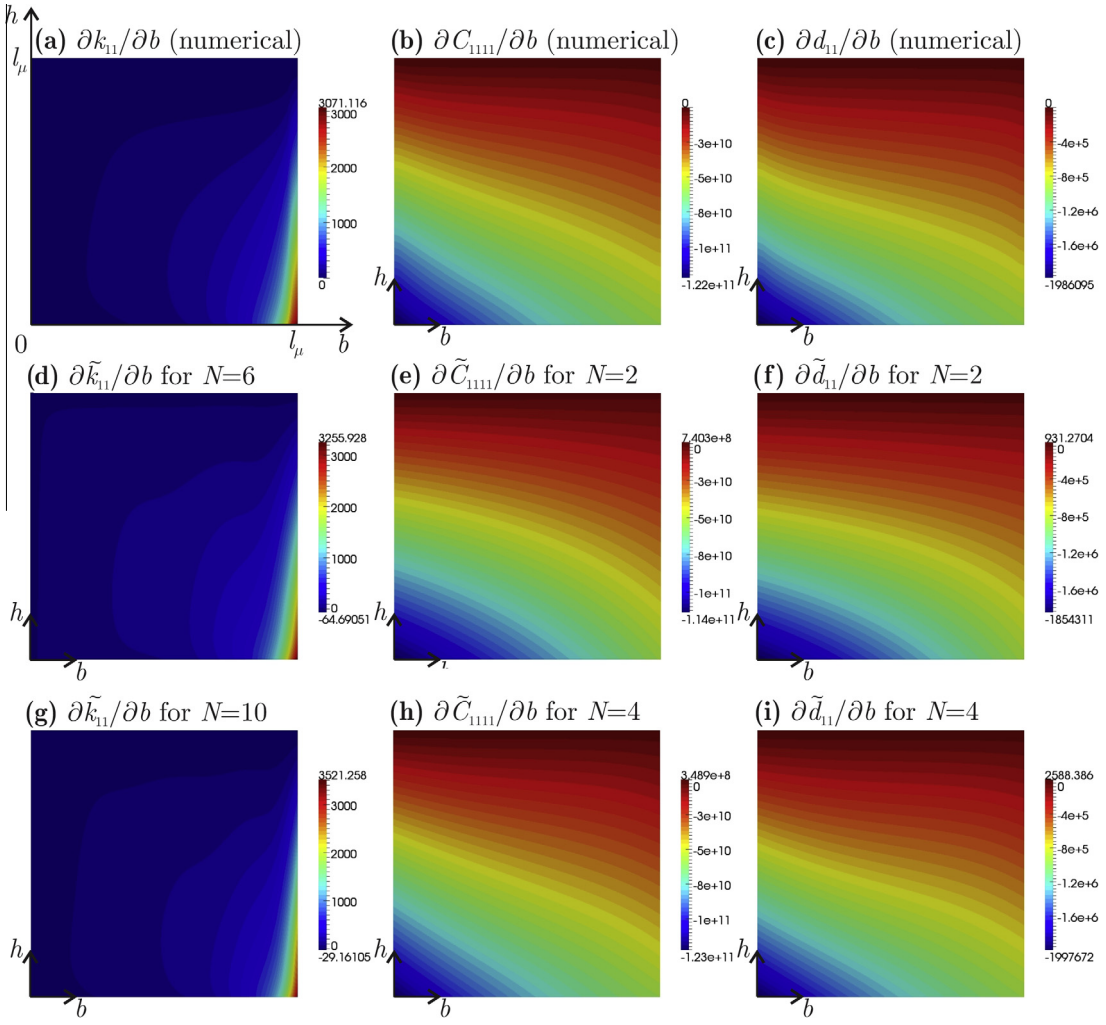

Fig. 9. Derivatives of effective properties as functions of b and h ($0 \leqslant b,\ h \leqslant l_\mu$): (a) numerical derivative $\partial k_{11}/\partial b$ in (W/(m^2 °C)); (b) numerical derivative $\partial C_{1111}/\partial b$ in (Pa/m); (c) numerical derivative $\partial d_{11}/\partial b$ in (Pa/(m °C)); (d)–(i) derivatives $\partial \tilde{k}_{11}/\partial b$, $\partial \tilde{C}_{1111}/\partial b$ and $\partial \tilde{d}_{11}/\partial b$, analytically computed from the polynomial approximation of the respective properties, for different degrees of the polynomials.

Table 5
Magnitude of the vertical displacement of the free end of the plate (v^{tip}) and total external work ($\mathbf{U}^T\mathbf{F}^{\text{tm}}$) for three different homogeneous microstructures.

Property	$b = h = 0$	$b = h = l_\mu/2$	$b = h = l_\mu$
v^{tip}	9.80 mm	15.26 mm	17.21 mm
$\mathbf{U}^T\mathbf{F}^{\text{tm}}$	9.709×10^4 Nm	1.839×10^5 Nm	2.171×10^5 Nm

$$\frac{\partial \mathcal{R}}{\partial P_i} = \left(\frac{\partial \mathbf{U}}{\partial P_i}\right)^T \mathbf{F}^{\text{tm}} + \mathbf{U}^T \frac{\partial \mathbf{F}^{\text{tm}}}{\partial P_i} = \mathbf{U}^T \left(2\frac{\partial \mathbf{F}^{\text{tm}}}{\partial P_i} - \frac{\partial \mathbf{K}^{\text{m}}}{\partial P_i}\mathbf{U}\right) \tag{54}$$

with $\partial \mathbf{U}/\partial P_i$, $\partial \mathbf{K}^{\text{m}}/\partial P_i$, and $\partial \mathbf{F}^{\text{tm}}/\partial P_i$ given by Eqs. (38), (40) and (41), respectively. As mentioned in Section 4.2.1, the computation of the sensitivity according to Eq. (54) is more expensive than in the case of fixed thermal expansion, because of the non-sparsity of the vector $\partial \mathbf{F}^{\text{tm}}/\partial P_i$.

Let us consider the plate with three different homogeneous microstructures: $b = h = 0$ (i.e., fully made of M^{matrix}=steel), $b = h = l_\mu/2$ and $b = h = l_\mu$ (i.e., fully made of M^{layer}=copper). The external work done by the thermal loads shown in Fig. 3(a), for these three cases, is listed in Table 5. Fig. 10 shows the sensitivity of this response to changes in the microstructure throughout the macroscopic domain.

6.5. Sensitivity of the macroscopic response to microstructural changes

Alternatively, the response of the thermally-loaded plate can be characterized by the magnitude of the X_2-displacement of the node located at $X_1 = L$, $X_2 = 0$ (lower right corner), say v^{tip}, i.e.

$$\mathcal{R}(\mathbf{U}, \mathbf{T}) = v^{\text{tip}}. \tag{55}$$

Let j be the degree of freedom corresponding to the X_2-displacement of such node. According to the X_1-X_2 frame adopted in Fig. 3(a), it holds that $U_j < 0$ for $T^{\text{top}} > T^{\text{bottom}}$, hence $v^{\text{tip}} = |U_j| = -U_j$. Using Eq. (56), the sensitivity of v^{tip} to microstructural changes is

$$\frac{\partial \mathcal{R}}{\partial P_i} = -\frac{\partial U_j}{\partial P_i} = \mathbf{j}^{\text{m}} \cdot \mathbf{s}_i^{\text{m}}, \quad \text{for given } j, \tag{56}$$

where $\mathbf{j}^{\text{m}}$ is the jth row of the inverse of the matrix $\mathbf{K}^{\text{m}}$. Once again, the sensitivity analysis is more expensive than in the case of prescribed thermal expansion, since the vector $\mathbf{s}_i^{\text{m}}$, Eq. (39), inherits the non-sparsity of $\partial \mathbf{F}^{\text{tm}}/\partial P_i$.

The values of v^{tip} for three different homogeneous microstructures are listed in Table 5. Fig. 11 shows the sensitivity of v^{tip} to microstructural changes for these three cases.

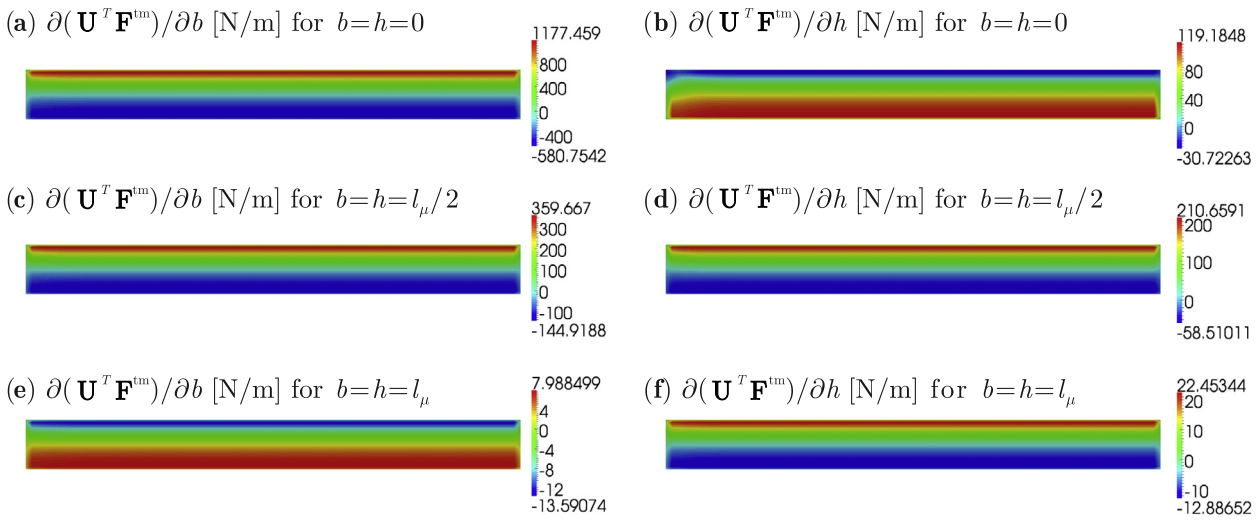

Fig. 10. Sensitivity of the total external work to microstructural changes, for three different homogeneous microstructures ($b=h=0$, $b=h=l_\mu/2$, and $b=h=l_\mu$).

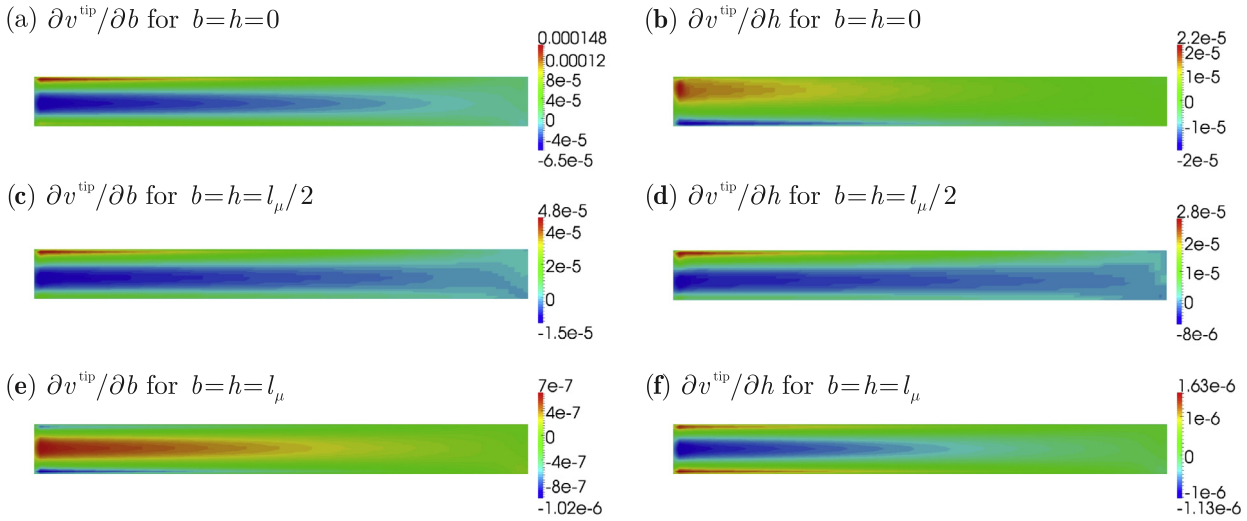

Fig. 11. Sensitivity of the vertical displacement of the lower free corner of the plate to microstructural changes, for different homogeneous microstructures ($b=h=0$, $b=h=l_\mu/2$, $b=h=l_\mu$).

6.5.1. Increasing the compliance/stiffness of the plate

The compliance of the considered thermally-loaded plate increases or decreases as $\mathcal{R}$ (given either by Eq. (53) or by Eq. (55)) increases or decreases, respectively. Then, the compliance of the plate can be modified by modifying P_i according to the sign of $\partial R/\partial P_i$.

From the finite difference approximation

$$\frac{\partial \mathcal{R}}{\partial P_i} \approx \frac{\mathcal{R}^{new}-\mathcal{R}}{P_i^{new}-P_i}, \tag{57}$$

we can update P_i using the expression

$$P_i^{new} = P_i + \left(\frac{\partial \mathcal{R}}{\partial P_i}\right)^{-1}(\mathcal{R}^{new}-\mathcal{R}), \tag{58}$$

subject to the constraint

$$0 \leqslant P_i^{new} \leqslant l_\mu. \tag{59}$$

Further, since the RVE at $\mathbf{X}_\alpha$ is fully made of M^{matrix} if either $P_{2\alpha-1} \equiv b_\alpha = l_\mu$ (irrespectively of the value of h_α) or $P_{2\alpha} \equiv h_\alpha = l_\mu$ (irrespectively of the value of b_α), two additional constraints arise:

$$P_{2\alpha-1}^{new} = l_\mu \quad \text{if } P_{2\alpha}^{new} = l_\mu, \tag{60}$$

$$P_{2\alpha}^{new} = l_\mu \quad \text{if } P_{2\alpha-1}^{new} = l_\mu. \tag{61}$$

Let us consider for instance the plate with a homogeneous microstructure $P_i = b = h = l_\mu/2$. Seeking for a more compliant plate, we adopt $\Delta\mathcal{R} = \mathcal{R}^{new} - \mathcal{R}$ positive and large enough such that Eq. (58) reduces to:

$$P_i^{new} = \begin{cases} 0 & \text{if } \partial\mathcal{R}/\partial P_i < 0 \\ l_\mu/2 & \text{if } \partial\mathcal{R}/\partial P_i = 0 \\ l_\mu & \text{if } \partial\mathcal{R}/\partial P_i > 0 \end{cases} \quad \text{to increase compliance,} \tag{62}$$

subject to the constraints (60) and (61).

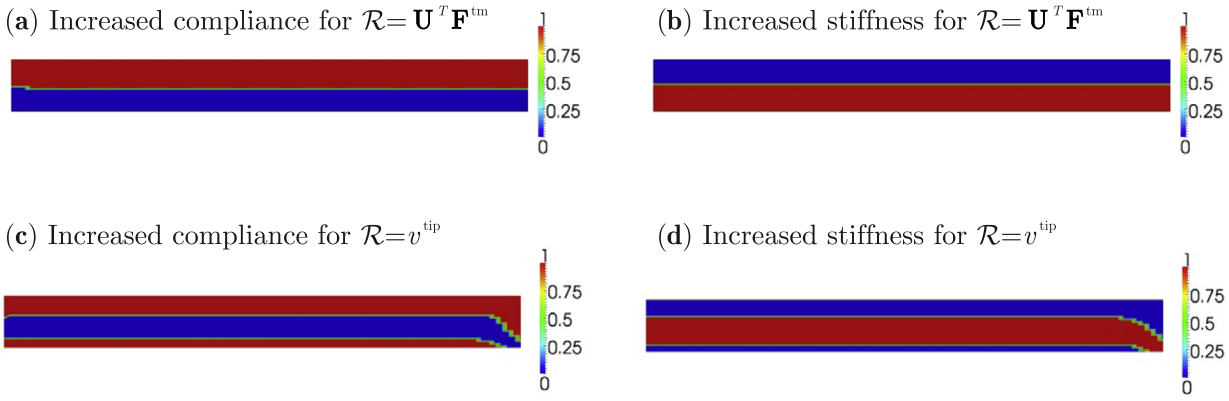

Fig. 12. Distribution of material for increased compliance (left) and stiffness (right) using sensitivity analysis, starting from $b = h = l_\mu/2$. The color-bars depict $0 \leqslant b/l_\mu = h/l_\mu \leqslant 1$.

Considering the macroscopic response given by $\mathcal{R} = \mathbf{U}^T\mathbf{F}^{tm}$, the sensitivities $\partial\mathcal{R}/\partial b$ and $\partial\mathcal{R}/\partial h$ when $b = h = l_\mu/2$ all over the plate are those shown in Fig. 10(c) and (d), respectively. As apparent from these figures, both derivatives have equal sign throughout the plate. Consequently, the Eq. (62) gives an identical solution for b and h, which is shown in Fig. 12(a). It consists of an upper layer of pure M^{layer} and a lower layer of pure M^{matrix}. In this case, the external work is $\mathbf{U}^T\mathbf{F}^{tm} = 2.704 \times 10^5$ Nm, that is 25% greater than the external work in the case of the plate completely made of M^{layer} (see Table 5), which is the material with the lower stiffness.

For $\mathcal{R} = v^{tip}$, $\partial\mathcal{R}/\partial b$ and $\partial\mathcal{R}/\partial h$ for $b = h = l_\mu/2$ throughout the plate are shown in Fig. 11(c) and (d), respectively. Once again, both derivatives have the same sign all over the plate. Therefore, Eq. (62) gives the same solution for the distribution of b and h, which is shown in Fig. 12(c). In this case, the solution consists of three layers: a core of M^{matrix} and upper and lower layers of M^{layer}. The maximum deflection of this plate is $v^{tip} = 22.96$ mm, that is 33% greater than the maximum deflection of the plate fully made of M^{layer} (see Table 5).

Analogously, to increase the stiffness (i.e., to decrease the compliance of the plate), we adopt $\Delta\mathcal{R} = \mathcal{R}^{new} - \mathcal{R}$ negative and large enough, such that Eq. (58) reduces to

$$P_i^{new} = \begin{cases} l_\mu & \text{if } \partial\mathcal{R}/\partial P_i < 0 \\ l_\mu/2 & \text{if } \partial\mathcal{R}/\partial P_i = 0 \\ 0 & \text{if } \partial\mathcal{R}/\partial P_i > 0 \end{cases} \quad \text{to increase stiffness,} \tag{63}$$

subject to the constraints (60) and (61).

For $\mathcal{R} = \mathbf{U}^T\mathbf{F}^{tm}$, Eq. (63) gives rise to the solution shown in Fig. 12(b), consisting of an upper layer of pure M^{matrix} and a lower layer of pure M^{layer}. In this case, the external work is $\mathbf{U}^T\mathbf{F}^{tm} = 4.939 \times 10^4$ Nm, which is sensibly smaller than the external work in the case of the plate fully made of M^{matrix} (see Table 5), which is the stiffer material.

For $\mathcal{R} = v^{tip}$, the solution of Eq. (63) is shown in Fig. 12(d): a plate with a core of M^{matrix} and upper and lower layers of M^{layer}. The maximum deflection of a such a plate is $v^{tip} = 6.02$ mm, which is considerably smaller than v^{tip} for the plate made of M^{matrix} (see Table 5).

7. Conclusions

In this work, we present a methodology for the sensitivity analysis of the thermomechanical response of macroscopic bodies with variable microstructure. The response of the body at the macroscale, influenced by the microstructure, has been analyzed using a semi-concurrent multiscale approach. Therefore, this evaluation requires the solution of a microscopic problem at each integration point, which makes the computation hardly affordable.

We propose to address this challenge for the wide range of "quantitatively characterized" materials by performing the microscale analysis in an offline stage. To this end, recourse is made to the response surface methodology in order to define the effective thermal and mechanical properties as polynomial functions of the parameters that define the microstructure. In this way, the sensitivities of the effective material properties to microstructural changes are also defined by polynomial functions.

Note that, given the microstructure distribution throughout the body, the response surface methodology allows us to predefine all the material properties as known functions of positions. Then, the determination of the macroscopic response becomes a standard problem at the macroscopic scale, which can be solved using most of the available FEM codes.

The reduction of the starting fully-online multiscale problem to one at the macroscale implies a huge reduction in computational time. This fact is a crucial contribution of this work, since it enables the optimal design of complex structures made of "quantitatively characterized" materials with spatially variable microstructure. The proposed methodology makes now affordable to solve a multiscale problem at each iteration of an optimization process. Actually, this is the purpose of our future works.

Acknowledgments

The first author has received funding from the Council for Scientific and Technical Research of Argentina (CONICET) through the research project PIP 2012–2014 GI-1105: "Computational Simulation of Multiphysics Problems. Application to Metal Solidification and Microelectromechanical Devices".

The research leading to these results has also received funding from the European Research Council under the Seventh Framework Program (FP/2007-2013)/ERC Grant Agreement n. 320815 (ERC Advanced Grant Project "COMP-DES-MAT: Advanced Tools for Computational Design of Engineering Materials").

Appendix A. Thermomechanical computational homogenization based on variational principles

This Appendix describes the main aspects characterizing the homogenization methodology adopted in this work: the

variational formulation and the equations governing the scale transition technique. Similar multiscale techniques for mechanical problems have been presented by Feyel and Chaboche (2000), Miehe and Koch (2002) and de Souza Neto and Feijóo (2008). Additional aspects of the methodology can be seen there.

A.1. Scale transition technique

Let us consider a material whose microstructure is statistically homogeneous at the macroscale. Every point $\mathbf{X} \in \Omega$ has associated a given RVE, which is identified with the domain Ω_μ having a piecewise smooth boundary Γ_μ and outward normal unit vector $\mathbf{n}_\mu$, see Fig. 1. Hereafter, $(\cdot)_\mu$ denotes an object described in Ω_μ. The *separation scale condition* is also assumed: the characteristic length of the RVE, denoted l_μ, is much less than the corresponding characteristic size, say L, of the macro scale domain: $l_\mu \ll L$.

A.1.1. Thermal problem

The thermal response at $\mathbf{X} \in \Omega$ is computed by means of a homogenization technique on the associated RVE, which domain is denoted Ω_μ. The temperature field in Ω_μ is defined as the sum of three contributions, as follows:

$$T_\mu = T + \nabla_{\mathbf{X}} T \cdot \mathbf{y} + \tilde{T}_\mu, \tag{AI-1}$$

where T and $\nabla_{\mathbf{X}} T$ are given inputs defined from the macroscale analysis, and $\tilde{T}_\mu$ is the micro-fluctuation of the temperature field.

From Eq. (AI-1), the temperature gradient is

$$\nabla_{\mathbf{y}} T_\mu = \nabla_{\mathbf{X}} T + \nabla_{\mathbf{y}} \tilde{T}_\mu. \tag{AI-2}$$

Using the Fourier's law, the heat flux vector $\mathbf{q}_\mu$ at the microscale is

$$\mathbf{q}_\mu = -\mathbf{k}_\mu \nabla_{\mathbf{y}} T_\mu, \tag{AI-3}$$

where the conductivity tensor $\mathbf{k}_\mu = \mathbf{k}_\mu(\mathbf{y})$ is given for each material component at the microscopic scale.

Consistent formulations for scale transition procedures should satisfy specific constraints between fields described at the macro and microscopic domains. Accordingly, we postulate two basic *admissibility requirements* between both descriptions, considered as fundamental hypotheses of our approach: (i) the *thermal admissibility* and (ii) the *energetic admissibility*. Requirement (i) fixes the minimal consistent boundary conditions to be imposed on the RVE problem, while requirement (ii) determines a heat balance equation at the micro scale, as well as the homogenization formula for the macroscopic heat flux vector. Both requirements are further discussed below.

A.1.1.1. Thermal admissibility requirement. This requirement imposes the identity between the temperature gradient at the macroscale and the volumetric average of the temperature gradient at the microscale, i.e.

$$\nabla_{\mathbf{X}} T = \frac{1}{|\Omega_\mu|} \int_{\Omega_\mu} \nabla_{\mathbf{y}} T_\mu \mathrm{d}V_\mu, \tag{AI-4}$$

where $|\Omega_\mu|$ is the volume of Ω_μ. Considering $\nabla_{\mathbf{y}} T_\mu$ given by Eq. (AI-2) and using the Gauss's theorem, Eq. (AI-4) yields

$$\int_{\Gamma_\mu} \tilde{T}_\mu \mathbf{n}_\mu \mathrm{d}S_\mu = \mathbf{0}, \tag{AI-5}$$

which introduces a constraint on the temperature micro-fluctuation field at the RVE. This constraint is the minimum one to be imposed on $\tilde{T}_\mu$ in order to define an admissible micro-fluctuation field.

A multiscale model that adopts temperature micro-fluctuation fields satisfying Eq. (AI-5) is called *minimally constrained* thermal multiscale sub-model. Alternative sub-models using micro-fluctuation fields with additional constraints can be postulated. Typical choices are: *Taylor* sub-model or rule of mixtures ($\tilde{T}_\mu$ is null in Ω_μ), *linear* sub-model ($\tilde{T}_\mu$ is null on Γ_μ) or *periodic* sub-model ($\tilde{T}_\mu$ is periodic on sub-boundaries of Γ_μ with opposite normal vectors).

The vector space $\mathcal{T}_\mu$ that collects all admissible functions $\tilde{T}_\mu$ is defined as

$$\mathcal{T}_\mu = \left\{ v(\mathbf{y}) \,|\, v \in \mathcal{H}^1(\Omega_\mu) \quad \text{and} \quad \int_{\Gamma_\mu} v(\mathbf{y}) \mathbf{n}_\mu \mathrm{d}S_\mu = \mathbf{0} \right\}. \tag{AI-6}$$

In this case, $\mathcal{T}_\mu$ defines also the vector space for the thermally admissible virtual actions in temperature micro-fluctuations at the microscale.

A.1.1.2. Energetic admissibility requirement. We postulate the following variational sentence:

$$\mathbf{q} \cdot \nabla_{\mathbf{X}} \hat{T} = \frac{1}{|\Omega_\mu|} \int_{\Omega_\mu} \mathbf{q}_\mu \cdot \nabla_{\mathbf{y}} \hat{T}_\mu \mathrm{d}V_\mu \tag{AI-7}$$

for all $\nabla_{\mathbf{X}} \hat{T}$ and $\nabla_{\mathbf{y}} \hat{T}_\mu$ related by the constraint (AI-4).

Considering $\nabla_{\mathbf{y}} T_\mu$ as given by Eq. (AI-2), the fulfillment of the variational expression (AI-7) necessarily implies two consequences, namely:

1. the homogenization formula for the heat flux vector:

$$\mathbf{q} = \frac{1}{|\Omega_\mu|} \int_{\Omega_\mu} \mathbf{q}_\mu \mathrm{d}V_\mu; \tag{AI-8}$$

2. the heat balance equation at the RVE-level, which is enunciated as: given $\nabla_{\mathbf{X}} T$, find $\tilde{T}_\mu \in \mathcal{T}_\mu$ such that:

$$\int_{\Omega_\mu} \mathbf{q}_\mu \cdot \nabla_{\mathbf{y}} \hat{\tilde{T}}_\mu \mathrm{d}V_\mu = 0, \quad \forall \hat{\tilde{T}}_\mu \in \mathcal{T}_\mu. \tag{AI-9}$$

A.1.2. Mechanical problem

Similar to the thermal field T_μ, Eq. (AI-1), the displacement field $\mathbf{u}_\mu(\mathbf{y})$ on Ω_μ is defined as the sum of three contributions:

$$\mathbf{u}_\mu = \mathbf{u} + \boldsymbol{\varepsilon} \cdot \mathbf{y} + \tilde{\mathbf{u}}_\mu, \tag{AI-10}$$

where $\mathbf{u}$ and $\boldsymbol{\varepsilon}$ are given inputs from the macroscale, and $\tilde{\mathbf{u}}_\mu$ is the displacement micro-fluctuation field in Ω_μ. Then, the linear strain tensor on the microscale, defined in the conventional form, is

$$\boldsymbol{\varepsilon}_\mu = \nabla^s_{\mathbf{y}} \mathbf{u}_\mu = \boldsymbol{\varepsilon} + \underbrace{\nabla^s_{\mathbf{y}} \tilde{\mathbf{u}}_\mu}_{\tilde{\boldsymbol{\varepsilon}}_\mu}, \tag{AI-11}$$

$\tilde{\boldsymbol{\varepsilon}}_\mu$ being the strain micro-fluctuation tensor.

Let us assume that the mechanical behavior of each microcomponent obeys a linear thermoelastic law:

$$\boldsymbol{\sigma}_\mu = \mathbf{C}_\mu \boldsymbol{\varepsilon}_\mu + \mathbf{d}_\mu (T_\mu - T^0), \tag{AI-12}$$

where $\mathbf{C}_\mu$ is the tensor of elastic moduli and $\mathbf{d}_\mu$ is the stress increment per unit of temperature, which are both of them given properties of the microcomponents; T^0 denotes the temperature for zero-thermal stress, assumed to be common to all the microcomponents.

Considering that T_μ, as given by Eq. (AI-1), satisfies

$$T_\mu = T + \mathcal{O}(l_\mu / L), \tag{AI-13}$$

where $l_\mu / L \ll 1$ according to the separation scale condition, we further assume that

$$T_\mu - T^0 \approx T - T^0. \tag{AI-14}$$

Therefore, the dependence of $\boldsymbol{\sigma}_\mu$ on the temperature micro-fluctuation field can be disregarded in the constitutive law at the microscopic scale, Eq. (AI-12), which finally takes the form

$$\boldsymbol{\sigma}_\mu = \mathbf{C}_\mu \boldsymbol{\varepsilon}_\mu + \mathbf{d}_\mu (T - T^0). \tag{AI-15}$$

Thanks to this assumption, the classical thermoelastic constitutive Eq. (12) is recovered at the macroscopic scale.

Like in the thermal problem, additional constraints have to be imposed on the mechanical problem for a correct definition of the scale transition procedure. Analogously, we postulate two *mechanical admissibility requirements*: (i) the *kinematic admissibility* and (ii) the *power admissibility*. Requirement (i) provides consistent boundary conditions for the RVE, while requirement (ii) provides the variational equilibrium problem on the microscale along together with the corresponding homogenization formula for the macroscopic stress tensor $\boldsymbol{\sigma}$, as discussed in the following paragraphs.

A.1.3. Kinematic admissibility requirement

It imposes the equivalence between the strain $\boldsymbol{\varepsilon}$ at the macroscale and the volumetric average of the strain $\boldsymbol{\varepsilon}_\mu$ at the microscale, i.e.

$$\boldsymbol{\varepsilon} = \frac{1}{|\Omega_\mu|}\int_{\Omega_\mu} \boldsymbol{\varepsilon}_\mu \mathrm{d}V_\mu. \tag{AI-16}$$

In view of Eq. (AI-11), and using the Gauss's theorem, Eq. (AI-16) can be rewritten as

$$\int_{\Gamma_\mu} \tilde{\mathbf{u}}_\mu \otimes^s \mathbf{n}_\mu \mathrm{d}S_\mu = \mathbf{0} \tag{AI-17}$$

and represents the minimum constraint to be imposed on the field $\tilde{\mathbf{u}}_\mu$ in order to satisfy the kinematic admissibility condition. A multiscale (mechanical) model satisfying (AI-17) is a *minimally constrained* kinematical (mechanical) multiscale sub-model (de Souza Neto and Feijóo, 2008). Alternative submodels with additional kinematical constraints on the displacement micro-fluctuation field can be postulated. Typical choices are: *Taylor* sub-model or rule of mixtures ($\tilde{\mathbf{u}}_\mu$ is null in Ω_μ), *linear* sub-model ($\tilde{\mathbf{u}}_\mu$ is null on Γ_μ) or *periodic* sub-model ($\tilde{\mathbf{u}}_\mu$ is periodic on boundary parts having opposite normal vectors).

The vector space $\mathcal{U}_\mu$ that collects all admissible functions $\tilde{\mathbf{u}}_\mu$ is defined as

$$\mathcal{U}_\mu = \left\{ \mathbf{v}(\mathbf{y}) \,|\, \mathbf{v} \in \mathcal{H}^1(\Omega_\mu) \text{ and } \int_{\Gamma_\mu} \mathbf{v}(\mathbf{y}) \otimes^s \mathbf{n}_\mu \mathrm{d}S_\mu = \mathbf{0} \right\}. \tag{AI-18}$$

Note that $\mathcal{U}_\mu$ coincides with the space of kinematically admissible virtual actions in displacement micro-fluctuations.

A.1.4. Power admissibility requirement

This is the well-known Hill-Mandel principle of macrohomogeneity, which imposes the following identity:

$$\boldsymbol{\sigma} \cdot \hat{\boldsymbol{\varepsilon}} = \frac{1}{|\Omega_\mu|}\int_{\Omega_\mu} \boldsymbol{\sigma}_\mu \cdot \hat{\boldsymbol{\varepsilon}}_\mu \mathrm{d}V_\mu \tag{AI-19}$$

for all the virtual fields $\hat{\boldsymbol{\varepsilon}}$ and $\hat{\boldsymbol{\varepsilon}}_\mu$ related by the constraint (AI-16). Two consequences are derived from this identity, namely:

1. the homogenization formula for the stress tensor:

$$\boldsymbol{\sigma} = \frac{1}{|\Omega_\mu|}\int_{\Omega_\mu} \boldsymbol{\sigma}_\mu \mathrm{d}V_\mu; \tag{AI-20}$$

2. the mechanical equilibrium problem at the RVE-level, which is enunciated as: given $T(\mathbf{X})$ and $\boldsymbol{\varepsilon}(\mathbf{X})$, find $\tilde{\mathbf{u}}_\mu \in \mathcal{U}_\mu$ such that:

$$\int_{\Omega_\mu} \boldsymbol{\sigma}_\mu \cdot \nabla^s_{\mathbf{y}} \hat{\tilde{\mathbf{u}}}_\mu \mathrm{d}V_\mu = \mathbf{0}, \quad \forall \hat{\tilde{\mathbf{u}}}_\mu \in \mathcal{U}_\mu. \tag{AI-21}$$

A.1.5. Effective thermal conductivity tensor

After introducing expressions (AI-2) in (AI-3), and the resulting expression into (AI-8), we obtain the effective thermal conductivity tensor

$$\mathbf{k} = \frac{\partial \mathbf{q}}{\partial(\nabla_{\mathbf{X}} T)} = \overline{\mathbf{k}} + \tilde{\mathbf{k}} \tag{AI-22}$$

with

$$\overline{\mathbf{k}} = \frac{1}{|\Omega_\mu|}\int_{\Omega_\mu} \mathbf{k}_\mu \mathrm{d}V_\mu, \tag{AI-23}$$

$$\tilde{\mathbf{k}} = \left[\frac{1}{|\Omega_\mu|}\int_{\Omega_\mu} \mathbf{e}_i \cdot \left(\mathbf{k}_\mu \nabla_{\mathbf{y}} (\nabla_{\nabla T} \tilde{T}_\mu)_j \right) \mathrm{d}V_\mu \right] \mathbf{e}_i \otimes \mathbf{e}_j, \tag{AI-24}$$

where $\mathbf{e}_i$ is the ith vector of the canonical basis in $\mathbb{R}^3$, and

$$(\nabla_{\nabla T} \tilde{T}_\mu)_j \doteq \frac{\partial \tilde{T}_\mu}{\partial(\nabla_{\mathbf{X}} T)} \cdot \mathbf{e}_j \tag{AI-25}$$

is computed after solving the linear problem

$$\int_{\Omega_\mu} \mathbf{k}_\mu \nabla_{\mathbf{y}} (\nabla_{\nabla T} \tilde{T}_\mu)_j \cdot \nabla_{\mathbf{y}} \hat{\tilde{T}}_\mu \mathrm{d}V_\mu = -\int_{\Omega_\mu} \mathbf{k}_\mu \mathbf{e}_j \cdot \nabla_{\mathbf{y}} \hat{\tilde{T}}_\mu \mathrm{d}V_\mu, \quad \forall \hat{\tilde{T}}_\mu \in \mathcal{T}_\mu. \tag{AI-26}$$

A.1.5.1. Effective elasticity and thermal stress tensor. By replacing Eq. (AI-11) in Eq. (AI-15), and the resulting expression in (AI-20), the effective elasticity tensor $\mathbf{C}$ is

$$\mathbf{C} = \frac{\partial \boldsymbol{\sigma}}{\partial \boldsymbol{\varepsilon}} = \overline{\mathbf{C}} + \tilde{\mathbf{C}} \tag{AI-27}$$

with

$$\overline{\mathbf{C}} = \frac{1}{|\Omega_\mu|}\int_{\Omega_\mu} \mathbf{C}_\mu \mathrm{d}V_\mu, \tag{AI-28}$$

$$\tilde{\mathbf{C}} = \left[\frac{1}{|\Omega_\mu|}\int_{\Omega_\mu} (\mathbf{e}_i \otimes \mathbf{e}_j) \cdot \left(\mathbf{C}_\mu \nabla^s_{\mathbf{y}} (\nabla_\varepsilon \tilde{\mathbf{u}}_\mu)_{kl} \right) \mathrm{d}V_\mu \right] \mathbf{e}_i \otimes \mathbf{e}_j \otimes \mathbf{e}_k \otimes \mathbf{e}_l, \tag{AI-29}$$

where

$$(\nabla_\varepsilon \tilde{\mathbf{u}}_\mu)_{kl} \doteq \frac{\partial \tilde{\mathbf{u}}_\mu}{\partial \boldsymbol{\varepsilon}} \cdot (\mathbf{e}_k \otimes \mathbf{e}_l) \tag{AI-30}$$

is the solution of the linear problem

$$\int_{\Omega_\mu} \mathbf{C}_\mu \nabla^s_{\mathbf{y}} (\nabla_\varepsilon \tilde{\mathbf{u}}_\mu)_{kl} \cdot \nabla^s_{\mathbf{y}} \hat{\tilde{\mathbf{u}}}_\mu \mathrm{d}V_\mu = -\int_{\Omega_\mu} \mathbf{C}_\mu (\mathbf{e}_k \otimes \mathbf{e}_l) \cdot \nabla^s_{\mathbf{y}} \hat{\tilde{\mathbf{u}}}_\mu \, \mathrm{d}V_\mu, \quad \forall \hat{\tilde{\mathbf{u}}}_\mu \in \mathcal{U}_\mu. \tag{AI-31}$$

On its turn, introducing the constitutive Eq. (AI-15) at the microscale into the homogenization formula (AI-20) for $\boldsymbol{\sigma}$ and differentiating with respect to the macroscopic temperature, we obtain the effective stress tensor increment per unit temperature

$$\mathbf{d} = \frac{\partial \boldsymbol{\sigma}}{\partial T} = \overline{\mathbf{d}} + \tilde{\mathbf{d}} \tag{AI-32}$$

with

$$\overline{\mathbf{d}} = \frac{1}{|\Omega_\mu|}\int_{\Omega_\mu} \mathbf{d}_\mu dV_\mu, \tag{AI-33}$$

$$\tilde{\mathbf{d}} = \int_{\Omega_\mu} \mathbf{C}_\mu \nabla^s_{\mathbf{y}}(\nabla_T \tilde{\mathbf{u}}_\mu) dV_\mu, \tag{AI-34}$$

where $\nabla_T \tilde{\mathbf{u}}_\mu$is the solution of the linear equation

$$\int_{\Omega_\mu} \mathbf{C}_\mu \nabla^s_{\mathbf{y}}(\nabla_T \tilde{\mathbf{u}}_\mu) \cdot \nabla^s_{\mathbf{y}} \hat{\tilde{\mathbf{u}}}_\mu dV_\mu = -\int_{\Omega_\mu} \mathbf{d}_\mu \cdot \nabla^s_{\mathbf{y}} \hat{\tilde{\mathbf{u}}}_\mu dV_\mu, \quad \forall \hat{\tilde{\mathbf{u}}}_\mu \in \mathcal{U}_\mu. \tag{AI-35}$$

More details about the derivation, from a variational point of view, of the tangent operators **k**, **C** and **d**, can be found in the works of Michel et al. (1999) and Giusti et al. (2009).

References

Bendsøe, M.P., Sigmund, O., 2003. Topology Optimization. Theory, Methods, and Applications. Springer-Verlag.

Chen, J., Rungsiyakull, C., Li, W., Chen, Y., Swain, M., Li, Q., 2013. Multiscale design of surface morphological gradient for osseointegration. J. Mech. Behav. Biomed. Mater. 20, 387–397.

de Souza Neto, E.A., Feijóo, R.A., 2008. On the equivalence between spatial and material volume averaging of stress in large strain multi-scale solid constitutive models. Mech. Mater. 40, 803–811.

Feyel, F., Chaboche, J.L., 2000. FE-2 multiscale approach for modelling the elastoviscoplastic behaviour of long fibre SiC/Ti composite materials. Comput. Methods Appl. Mech. Eng. 183 (3), 309–330.

Fish, J., Ghouali, A., 2001. Multiscale analytical sensitivity analysis for composite materials. Int. J. Numer. Methods Eng. 50 (6), 1501–1520.

Giusti, S.M., Blanco, P.J., de Souza Neto, E.A., Feijóo, R.A., 2009. An assessment of the Gurson yield criterion by a computational multi-scale approach. Eng. Comput.: Int. J. Comput. Aided Eng. Software 26 (3), 281–301.

Hou, S., Li, Q., Long, S., Yang, X., Li, W., 2008. Multiobjective optimization of multi-cell sections for the crashworthiness design. Int. J. Impact Eng. 35, 1355–1367.

Kachanov, M., Sevostianov, I., 2005. On quantitative characterization of microstructures and effective properties. Int. J. Solids Struct. 42, 309–336.

Kamiński, M., 2009. Sensitivity and randomness in homogenization of periodic fiber-reinforced composites via the response function method. Int. J. Solids Struct. 46 (3), 923–937.

Kamiński, M., 2014. Design sensitivity analysis for the homogenized elasticity tensor of a polymer filled with rubber particles. Int. J. Solids Struct. 51 (3), 612–621.

Lund, E., Stegmann, J., 2005. On structural optimization of composite shell structures using a discrete constitutive parametrization. Wind Energy 8 (1), 109–124.

McDowell, D., Story, T., 1998. New directions in materials design science and engineering. Report, Workshop Sponsored by the U.S. National Science Foundation, Georgia Institute of Technology and Morehouse College, Atlanta, GA, USA.

Michel, J.C., Moulinec, H., Suquet, P., 1999. Effective properties of composite materials with periodic microstructure: a computational approach. Comput. Methods Appl. Mech. Eng. 172, 109–143.

Miehe, C., Koch, A., 2002. Computational micro-to-macro transitions of discretized microstructures undergoing small strains. Arch. Appl. Mech., 0939-1533 72 (4), 300–317.

Paulino, G.H., Silva, E.C.N., Le, C.H., 2009. Optimal design of periodic functionally graded composites with prescribed properties. Struct. Multidiscip. Optim. 38 (5), 469–489.

Rodrigues, H., Guedes, J.M., Bendsøe, M.P., 2002. Hierarchical optimization of material and structure. Struct. Multidiscip. Optim. 24 (1), 1–10.

Rungsiyakull, C., Li, Q., Sun, G., Li, W., Swain, M.V., 2010. Surface morphology optimization for osseointegration of coated implants. Biomaterials 31, 7196–7204.

Torquato, S., 2010. Optimal design of heterogeneous materials. Annu. Rev. Mater. Res. 40, 101–129.

Tsukrov, I., Kachanov, M., 2000. Effective moduli of an anisotropic material with elliptical holes of arbitrary orientational distribution. Int. J. Solids Struct. 37, 5919–5941.

Yin, H.M., Paulino, G.H., Buttlar, W.G., Sun, L.Z., 2007. Micromechanics-based thermoelastic model for functionally graded particulate materials with particle interactions. J. Mech. Phys. Solids 55 (1), 132–160.

Zienkiewicz, O.C., Taylor, R.L., 2000. The Finite Element Method,, .. The Basis, fifth ed., vol. 1. Butterworth-Heinemann.